CELL BIOLOGY

2′3′-cGAMP interactome identifies 2′3′-cGAMP/Rab18/FosB signaling in cell migration control independent of innate immunity

Yu Deng[1,2], Quentin Hahn[2], Le Yu[1,2], Zhichuan Zhu[1,2], Joshua A. Boyer[2], Jian Wang[3,4,5], Deyu Kong[6], Leiah M. Carey[1,2], Austin J. Hepperla[1,7,8], Jeremy M. Simon[1,7,8,9,10], Brenda Temple[2], Zhigang Zhang[1,11,12], Yanqiong Zhang[1,2], Charlene Santos[13], Jonathan E. Frank[14], Laura E. Herring[15], Xiaodong Wang[1,6], Nikolay V. Dokholyan[3,4,5], Sharon L. Campbell[1,2], Albert S. Baldwin[1], Blossom Damania[1,11,12], Qi Zhang[2], Pengda Liu[1,2]*

c-di-GAMP was first identified in bacteria to promote colonization, while mammalian 2′3′-cGAMP is synthesized by cGAS to activate STING for innate immune stimulation. However, 2′3′-cGAMP function beyond innate immunity remains elusive. Here, we report that 2′3′-cGAMP promotes cell migration independent of innate immunity. 2′3′-cGAMP interactome analysis identifies the small GTPase Rab18 as a 2′3′-cGAMP binding partner and effector in cell migration control. Mechanistically, 2′3′-cGAMP binds Rab18 to facilitate GTP loading and subsequent Rab18 activation, which further promotes FosB transcription in facilitating cell migration. Induced synthesis of endogenous 2′3′-cGAMP by intrabreast tumor bacterium *S. aureus* infection or low-dose doxorubicin treatment facilitates cell migration depending on the cGAS/cGAMP/Rab18/FosB signaling. We find that lovastatin induces Rab18 deprenylation that abolishes 2′3′-cGAMP recognition therefore suppressing cell migration. Together, our study reveals a previously unidentified 2′3′-cGAMP function in cell migration control via the 2′3′-cGAMP/Rab18/FosB signaling that provides additional insights into clinical applications of 2′3′-cGAMP.

INTRODUCTION

Cyclic mononucleotides [such as cyclic adenosine 3′,5′-monophosphate (cAMP)] play key roles as second messengers in bacteria and vertebrates (*1*). Cyclic dinucleotides serve as bacterial secondary messengers, where cyclic di-GMP (c-di-GMP) contributes to motility, biofilm formation, and virulence, while cyclic di-AMP (c-di-AMP) regulates sporulation, cell wall metabolism, and osmotic stress responses (*2*). A hybrid cyclic dinucleotide [cyclic GAMP (cGAMP)] was first discovered in bacteria to promote colonization and virulence (*3*) by binding an RNA riboswitch to promote gene expression (*4*). In mammals, 2′3′-cGAMP serves as an essential signaling messenger in nonspecific immunity (innate immunity) to defend against pathogens. Mechanistically, accumulation of cytosolic DNA from viral or bacterial infection, or derived from damaged genome or mitochondria, activates mammalian cGAS (cGAMP synthase) to generate 2′3′-cGAMP (*5*, *6*). 2′3′-cGAMP binds and activates stimulator of interferon genes (STING) on endoplasmic reticulum to promote type I interferon (IFN) production (*7*) and expression of antiviral/immunomodulatory genes (*8*). Recent therapies have sought to take advantage of its role in innate immunity, such as treating autoimmune diseases by blocking cGAMP production via cGAS inhibitors (*9*) or using cGAMP as an immune adjuvant to enhance antitumor effects of immune checkpoint blockade by stimulating immune cell function (*10*).

However, physiological roles of 2′3′-cGAMP in normal and pathological conditions beyond innate immunity remain poorly understood. Recently, in addition to STING, elongation factor 1-alpha 1 (EF1A1) was reported as another 2′3′-cGAMP downstream effector that 2′3′-cGAMP binding to EF1A1 suppresses protein translation (*11*). Given that multiple functions of non-cGAMP dinucleotides such as c-di-AMP were identified including regulating metabolic enzymes (*12*), K^+ homeostasis (*13*), osmotic homeostasis, and others through binding to distinct effectors (*14*), we thought to advance our understanding of 2′3′-cGAMP biology and function by identifying unknown mammalian 2′3′-cGAMP binding partners.

RESULTS

Intracellular 2′3′-cGAMP promotes cell migration in vitro

We first examined whether 2′3′-cGAMP treatment affected cell behaviors. Although addition of 2′3′-cGAMP to the cell culture media did not affect MDA-MB-231 cell proliferation (fig. S1, A and B), this treatment promoted MDA-MB-231 cell migration in vitro measured by transwell assays (*15*, *16*) that determine the number of cells capable of migrating across a membrane support (Fig. 1, A and B,

[1]Lineberger Comprehensive Cancer Center, The University of North Carolina at Chapel Hill, Chapel Hill, NC 27599, USA. [2]Department of Biochemistry and Biophysics, The University of North Carolina at Chapel Hill, Chapel Hill, NC 27599, USA. [3]Department of Pharmacology, Penn State College of Medicine, Hershey, PA 17033, USA. [4]Department of Biomedical Engineering, Pennsylvania State University, University Park, PA 17033, USA. [5]Department of Biochemistry and Molecular Biology, Penn State College of Medicine, Hershey, PA 17033, USA. [6]Center for Integrative Chemical Biology and Drug Discovery, Division of Chemical Biology and Medicinal Chemistry, Eshelman School of Pharmacy, The University of North Carolina at Chapel Hill, Chapel Hill, NC 27599, USA. [7]Carolina Institute for Developmental Disabilities, The University of North Carolina at Chapel Hill, Chapel Hill, NC 27599, USA. [8]UNC Neuroscience Center, The University of North Carolina at Chapel Hill, Chapel Hill, NC 27599, USA. [9]Department of Genetics, The University of North Carolina at Chapel Hill, Chapel Hill, NC 27599, USA. [10]Department of Data Science, Dana-Farber Cancer Institute Department of Biostatistics, Harvard T.H. Chan School of Public Health, Boston, MA 02115, USA. [11]Department of Microbiology and Immunology, University of North Carolina at Chapel Hill, Chapel Hill, NC 27599, USA. [12]University of North Carolina Center for AIDS Research, University of North Carolina at Chapel Hill, Chapel Hill, NC 27599, USA. [13]UNC Animal Studies Core Facility, The University of North Carolina at Chapel Hill, Chapel Hill, NC 27599, USA. [14]UNC Small Animal Imaging Core Facility, The University of North Carolina at Chapel Hill, Chapel Hill, NC 27599, USA. [15]UNC Proteomics Core Facility, Department of Pharmacology, The University of North Carolina at Chapel Hill, Chapel Hill, NC 27599, USA.
*Corresponding author. Email: pengda_liu@med.unc.edu

and fig. S1, C and D) by increasing intracellular 2′3′-cGAMP levels (Fig. 1C and fig. S1E). 2′3′-cGAMP treatment also increased intracellular 2′3′-cGAMP levels in T47D cells (fig. S1F) to promote T47D cell migration (fig. S1, G and H) although 2′3′-cGAMP did not activate STING/interferon regulatory factor 3 (IRF3) signaling (fig. S1I). Similarly, 2′3′-cGAMP facilitated migration of MDA-MB-453, MDA-MB-468, and mouse embryonic fibroblast (MEF) cells in vitro (Fig. 1, D and E). Notably, 2′3′-cGAMP alone in the absence of fetal bovine serum (FBS) retained its ability to promote migration of MDA-MB-231 cells (Fig. 1, F and G) and MEFs (fig. S1, J and K). Moreover, compared with 20% FBS as a characterized migration inducer in transwell assays, 2′3′-cGAMP exerted an additive effect to further promote FBS-driven cell migration (extended figs. S1, L and M). Together, these data suggest that 2′3′-cGAMP may promote cell migration.

Considering that 2′3′-cGAMP is not cell permissible, we next tested whether 2′3′-cGAMP treatment increased intracellular 2′3′-cGAMP levels to induce cell migration. To this end, we firstly profiled protein expression of reported 2′3′-cGAMP importers/transporters including LRRC8C (*17*, *18*), SLC46A2 (*19*), SLC19A1 (*20*, *21*), and the gap junction protein connexin 43 (*22*) and found that MDA-MB-231 cells were deficient in SLC19A1 expression but with decent expression of LRRC8C and SLC46A2 (fig. S1N). We depleted both LRRC8C and SLC46A2 by short hairpin RNAs (shRNAs; fig. S1O) and found that this led to substantially reduced 2′3′-cGAMP uptake (fig. S1P), which subsequently attenuated 2′3′-cGAMP–triggered MDA-MB-231 cell migration (fig. S1, Q and R). These data indicate that extracellular 2′3′-cGAMP was imported in MDA-MB-231 cells largely by LRRC8 and SLC46A2, and blocking 2′3′-cGAMP uptake impairs 2′3′-cGAMP–induced MDA-MB-231 cell migration. These data suggest that heightened levels of intracellular 2′3′-cGAMP likely contribute to increased cell migration.

Given that extracellular 2′3′-cGAMP is degraded by ENPP1 (ectonucleotide pyrophosphatase/phosphodiesterase 1) (*23*) into GMP and AMP, and AMP is further converted to adenosine (*24*), a molecule that has been reported to facilitate cell migration (*25*), we further examined whether 2′3′-cGAMP induced cell migration via adenosine signaling. We firstly treated MDA-MB-231 cells with adenosine and found that, consistent with previous reports (*25*), adenosine increased MDA-MB-231 cell migration (fig. S1, S and T). Notably, ENPP1 inhibition by ENPP1 inhibitor 1c showed an additive effect in further increasing 2′3′-cGAMP–triggered cell migration (fig. S1, U and V) accompanied by increased intracellular 2′3′-cGAMP levels (fig. S1W). Given that ENPP1 inhibition results in less adenosine production, these data suggest that ENPP1 inhibition–induced cell migration is largely through increasing intracellular 2′3′-cGAMP levels rather than adenosine accumulation. To further determine whether adenosine and its receptor A2B (*26*) play roles in cGAMP-induced cell migration, we depleted endogenous A2B in MDA-MB-231 cells (fig. S1X) and found that this did not notably affect intracellular 2′3′-cGAMP levels upon 2′3′-cGAMP treatment (fig. S1Y) and subsequent cell migration (fig. S1Z, z1). Similar observations were also obtained from MDA-MB-468 cells (fig. S1, z2 to z5). Furthermore, pharmacologically inhibiting A2B by MRS-1706 did not affect intracellular 2′3′-cGAMP levels upon 2′3′-cGAMP treatment (fig. S1, z6 and z7) and subsequent migration of both MDA-MB-231 and MDA-MB-468 cells (fig. S1, z8 and z9). These data collectively support that 2′3′-cGAMP promotes cell migration largely through increasing intracellular 2′3′-cGAMP levels. In addition to breast cancer cells, we also found that 2′3′-cGAMP promoted migration of colon cancer DLD-1 cells in vitro (fig. S1, z10 and z11).

Moreover, we used a nonhydrolysable 2′3′-cGAMP analog, 2′3′-cGAM(PS)2 (*23*), and observed even nanomolar scale of 2′3′-cGAM(PS)2 could trigger MDA-MB-231 cell migration (Fig. 1, Q and R). Compared with 2′3′-cGAMP, similar amount of 2′3′-cGAM(PS)2 triggered more robust MDA-MB-231 cell migration in the presence of FBS (fig. S1, z12 and z13), which was largely due to that cells uptake more 2′3′-cGAM(PS)2 than 2′3′-cGAMP (fig. S1z14). Considering that the only reported extracellular 2′3′-cGAMP degrader ENPP1 (*23*) is highly abundant in FBS, we further tested effects of comparable amounts of 2′3′-cGAMP and 2′3′-cGAM(PS)2 in regulating cell migration without FBS (and with no ENPP1). To this end, we observed that both 2′3′-cGAMP and 2′3′-cGAM(PS)2 potentiated cell migration (fig. S1, z15 and z16) because without ENPP1-mediated extracellular 2′3′-cGAMP degradation, comparable amounts of 2′3′-cGAMP and 2′3′-cGAM(PS)2 were uptake by cells to drive cell migration. Together, these data reinforce the notion that intracellular 2′3′-cGAMP promotes cell migration.

In addition to transwell assays, we also performed live-cell imaging, which further confirmed that MDA-MB-231 cells treated with 2′3′-cGAMP displayed enhanced cell movements (fig. S2, O to Q, and movies S1 and S2). Notably, information for all key reagents used in this study is summarized in Table 1.

2′3′-cGAMP promotes cell migration in vitro independent of STING

Considering that 2′3′-cGAMP binds STING to activate innate immunity, we next examined whether STING mediates 2′3′-cGAMP–induced cell migration. Depletion of STING in MDA-MB-231 cells by shRNAs (Fig. 1H) or single guide RNAs (sgRNAs; fig. S2A) had minimal effects on 2′3′-cGAMP–triggered cell migration either in the presence (Fig. 1, I and J) or absence of FBS (fig. S2, B to D). These data suggest that 2′3′-cGAMP promotes MDA-MB-231 cell migration independent of STING. Consistently, 2′3′-cGAMP also induced migration of MDA-MB-231 cells expressing a STING-R238A mutant [deficient in binding 2′3′-cGAMP (*27*)] to a comparable level as cells expressing STING–wild type (WT) (fig. S2, E to G). In addition, inactivating STING via H-151, a STING antagonist that disrupts STING palmitoylation, also showed negligible effects on 2′3′-cGAMP–induced MDA-MB-231 cell migration (fig. S2, H and I). On the other hand, activating STING in MEFs with a mouse STING-specific agonist DMXAA (fig. S2J) suppressed MEFs migration in vitro (fig. S2, K to N), suggesting that STING activation may suppress cell migration. Together, these data cumulatively suggest that 2′3′-cGAMP promotes cell migration in a STING-independent manner.

To further test whether 2′3′-cGAMP induces migration of multiple cell types and its dependence on STING/IRF3 innate immune signaling in these settings, we generated cGAS-depleted, STING-depleted, or IRF3-depleted MDA-MB-231, HeLa, BPH1, A498, and RCC10 cells. In all cells we examined, we observed that 2′3′-cGAMP treatment substantially increased cell migration (by live-cell imaging coupled quantification of migration) regardless of cGAS, STING, or IRF3 (fig. S2, R to z10). In addition, we also performed independent transwell assays to confirm observations using live-cell imaging that 2′3′-cGAMP promoted A498 cell migration independent of cGAS, STING, or IRF3 (fig. S2z11). These data further support the notion that 2′3′-cGAMP facilitates multiple types of cell migration in vitro independent of the canonical cGAS/STING/IRF3 innate immune signaling.

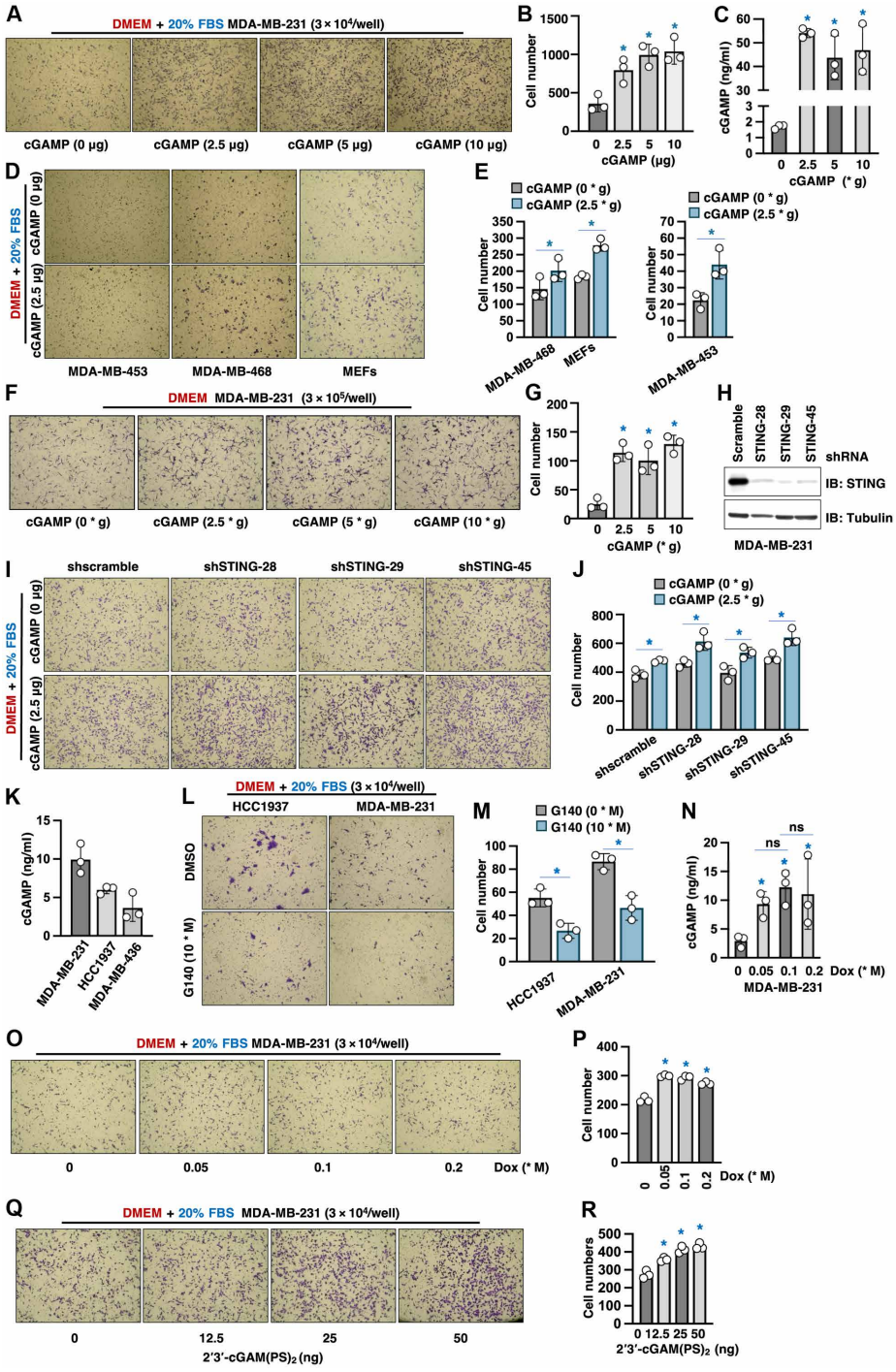

Fig. 1. 2′3′-cGAMP treatment promotes cell migration independent of STING. (**A**, **B**, **F**, **G**, **I**, **J**, **O**, **P**, **Q**, and **R**) Representative images of transwell assays using indicated numbers of indicated MDA-MB-231 cells under indicated conditions for 24 hours. Triplicates of (A), (F), (I), (Q), and (P) are quantified in (B), (G), (J), (P), and (R). Error bars were calculated as mean ± SD, $n = 3$ biological replicates. *$P < 0.05$ [one-way analysis of variance (ANOVA) test]. Where indicated, the amount of 2′3′-cGAMP is used in 300 μl of serum-free media in transwells. (**C**) 2′3′-cGAMP enzyme-linked immunosorbent assays (ELISAs) using 2 u 10^5 MDA-MB-231 cells from (A). (**D** and **E**) Representative images of transwell assays using 3×10^4 of indicated cells under indicated conditions for 24 hours and quantified in (E). Error bars were calculated as mean ± SD, $n = 3$ biological replicates. *$P < 0.05$ (one-way ANOVA test). Where indicated, 2.5 μg of 2′3′-cGAMP is used in 300 μl of serum-free media in transwells. (**H**) Immunoblot (IB) analysis of whole cell lysates (WCL) derived from indicated MDA-MB-231 cells. MDA-MB-231 cells were infected with either shscramble or shSTING viruses and selected in puromycin (1romyci to eliminate noninfected cells for 72 hours before cell collection. (**K**) 2′3′-cGAMP ELISA measurements using 10^6 indicated cells. (**L** and **M**) Representative images of transwell assays using 3 a 10^4 indicated cells treated with 10 M G140 for 24 hours and quantified in (M). Error bars were calculated as mean ± SD, $n = 3$. *$P < 0.05$ (one-way ANOVA test). (**N**) 2′3′-cGAMP ELISA measurements using 2×10^5 MDA-MB-231 cells treated with indicated doses of Dox for 24 hours. DMSO, dimethyl sulfoxide; ns, not significant.

Table 1. Key reagents used in this study. ATCC, American Type Culture Collection.

Reagent	Vendor	Catalog number
Antibodies		
Anti–HA-Tag antibody	Cell Signaling Technology	Catalog no. 3724
Anti-FosB antibody	Cell Signaling Technology	Catalog no. 2251
Anti-eEF1A1 antibody	Cell Signaling Technology	Catalog no. 2551
Anti–phospho-TBK1/NAK (Ser^{172}) antibody	Cell Signaling Technology	Catalog no. 5483
Anti-TBK1 antibody	Cell Signaling Technology	Catalog no. 51872
Anti-STING antibody (13647)	Cell Signaling Technology	Catalog no. 13647
Anti–phospho-STING (Ser^{366}) antibody	Cell Signaling Technology	Catalog no. 50907
Anti-IRF3 antibody	Cell Signaling Technology	Catalog no. 4302
Anti–phospho-IRF3 (Ser^{386}) antibody	Cell Signaling Technology	Catalog no. 37829
Anti–phospho-IRF3 (Ser^{396}) antibody	Cell Signaling Technology	Catalog no. 29047
Anti-cGAS antibody	Cell Signaling Technology	Catalog no. 83623
Anti–phospho-histone H2A.X (Ser^{139})	Cell Signaling Technology	Catalog no. 9718
Anti–GST-tag antibody	Santa Cruz Biotechnology	Catalog no. sc-459
Anti-Rab18 antibody	Santa Cruz Biotechnology	Catalog no. sc-393169
Anti–E-cadherin antibody	Santa Cruz Biotechnology	Catalog no. sc-212791
Anti-MMP9 antibody	Santa Cruz Biotechnology	Catalog no. sc-21733
Anti-Moesin antibody	Santa Cruz Biotechnology	Catalog no. sc-13122
Anti-SLUG antibody	Santa Cruz Biotechnology	Catalog no. sc-166476
Anti-MITF antibody	Santa Cruz Biotechnology	Catalog no. sc-515925
Anti-SNAI1 antibody	Santa Cruz Biotechnology	Catalog no. sc-271977
Anti-SPARC antibody	Santa Cruz Biotechnology	Catalog no. sc-398419
Anti-TIMP1 antibody	Santa Cruz Biotechnology	Catalog no. sc-365905
Anti–c-Jun antibody	Santa Cruz Biotechnology	Catalog no. sc-1694
Anti-rabbit IgG, HRP-linked antibody	Cell Signaling Technology	Catalog no. 7074
Anti-mouse IgG, HRP-linked antibody (7076)	Cell Signaling Technology	Catalog no. 7076
Polyclonal anti-Flag antibody	Sigma-Aldrich	Catalog no. F7425
Monoclonal anti-Flag antibody	Sigma-Aldrich	Catalog no. F-3165
Monoclonal anti-tubulin antibody	Sigma-Aldrich	Catalog no. T-5168
Anti-vinculin antibody	Santa Cruz Biotechnology	Catalog no. sc-25336
Anti-GFP antibody	Abcam	Catalog no. ab13970
Anti-LRRC8C antibody	Proteintech	Catalog no. 21601-1-AP
Anti-SLC19A1 antibody	Proteintech	Catalog no. 25958-1-AP
Anti-connexin43	Proteintech	Catalog no. 26980-1-AP
Anti-FAK	Proteintech	Catalog no. 12636-1-AP
Anti-SLC46A2	ABclonal	Catalog no. A15494
Anti-RAB27A antibody	Proteintech	Catalog no. 17817-1-AP
Anti-RAB3A antibody	Proteintech	Catalog no. 68052-2-Ig
Nucleotide stimulants		
ISD90	Eurofins Genomics	5′-TACAGATCTACTAGTGATCTATGACTGATCTG TACATGATCTACAT-ACAGATCTACTAGTGATCTATGACTGATCTGTACATGATCTACA-3′
Poly(I:C)	Sigma-Aldrich	Catalog no. P1530
Transfection reagents and antibiotics		
Polyethylenimine	Polysciences Inc.	Catalog no. 23866-1
Blasticidin	Sigma-Aldrich	Catalog no. 15205
Puromycin	Fisher BioReagents	Catalog no. 58-58-2
Hygromycin	Sigma-Aldrich	Catalog no. H3274
Gentamicin	Sigma-Aldrich	Catalog no. G1264

(*Continued*)

(*Continued*)

Reagent	Vendor	Catalog number
Experimental models: Cell lines		
MDA-MB-231	ATCC	
MDA-MB-453	ATCC	
MDA-MB-468	ATCC	
T47D	ATCC	
MEFs	ATCC	
MDA-MB-436	Q. Zhang (UT Southwestern)	
HCC1937	Q. Zhang (UT Southwestern)	
THP1	B. Damania (UNC)	
Human embryonic kidney 293T	ATCC	
Software and algorithms		
GraphPad Prism 8	Prism	
Other		
RNeasy Mini Kit	QIAGEN	Catalog no. 74106
iScrip Reverse Transcription Supermix for qRT-PCR	Bio-Rad	Catalog no. 170-8891
Taq universal SYBR green supermix	Bio-Rad	Catalog no. 172-5124
Protease inhibitor cocktail	Bimake	Catalog no. B14012
Phosphatase inhibitor cocktails A and B	Bimake	Catalog no. B15001-A/B15001-B
Lovastatin	TCI	Catalog no. L0214
Atorvastatin	TCI	Catalog no. A2476
Doxorubicin	Fisher BioReagents	Catalog no. BP2316-005
Biotin-2′3′-cGAMP	BioLOG	Catalog no. c197-001
3′2′-cGAMP	BioLOG	Catalog no. c238-005
3′3′-cGAMP	BioLOG	Catalog no. c117-001
2′3′-cGAMP	APExBio	Catalog no. 88362
GTP solution	Thermo Fisher Scientific	Catalog no. R0461
ActivX Desthiobiotin-GTP probe	Thermo Fisher Scientific	Catalog no. 88315
G140	InvivoGen	Catalog no. inh-g140
H-89	AdipoGen	Catalog no. 130964-39-5
Compound C	Milipore	Catalog no. 171260
Neutravidin agarose beads	Thermo Fisher Scientific	Catalog no. 29200
Glutathione agarose beads	GE Healthcare	Catalog no. 17-0756-05
Anti-HA agarose beads	Sigma-Aldrich	Catalog no. A-2095
Anti-Flag agarose beads	Sigma-Aldrich	Catalog no. A2220
cAMP	TCI	Catalog no. A2381
Alexa Fluor 594 phalloidin	Thermo Fisher Scientific	Catalog no. A12381
MRS-1706	MCE	Catalog no. 264623-53-9
Biotin-2′3′-cAMP	AAT Bioquest	Catalog no. 17105

Furthermore, we found that only 2′3′-cGAMP, but not other linkages of c-di-GAMP including 3′2′-cGAMP or 3′3′-cGAMP, potentiated MDA-MB-231 cell migration in vitro (fig. S3, A and B), although 3′3′-cGAMP could also be efficiently uptake by cells (fig. S3C). We next evaluated whether altering endogenous 2′3′-cGAMP levels affected cell migration. To this end, we observed a relatively higher level of endogenous 2′3′-cGAMP in MDA-MB-231 and HCC1937 cells (Fig. 1K). Inhibiting cGAS activity, therefore reducing endogenous cGAMP levels (fig. S3D) and subsequent canonical innate immune signaling (fig. S3E), by a characterized cGAS small-molecule catalytic inhibitor G140 (*28*), reduced migration of either of these two cell lines (Fig. 1, L and M). In addition, G140 treatment did not affect MDA-MB-231-cGAS-KO (knockout) cell migration (fig. S3, F and G) but retained its ability to suppress MDA-MB-231-STING-KO cell migration (fig. S3, H and I), further suggesting that 2′3′-cGAMP regulates cell migration independent of STING. On the other hand, increasing endogenous 2′3′-cGAMP levels via stimulation by ISD90 (an IFN stimulatory DNA fragment from *Listeria monocytogenes* used to mimic DNA viral infection; fig. S3J) promoted migration of WT (fig. S3, K to N) and STING-KO MDA-MB-231 cells (fig. S3, O to R). In addition, treatment of MDA-MB-231 cells with chemotherapeutic agents, such as low-dose doxorubicin (Dox), triggered

DNA damage (evidenced by increased g-H2Ax foci; fig. S3, S and T) to facilitate cGAS micronuclei recruitment (fig. S3, U and V). This led to cGAS activation and subsequent 2′3′-cGAMP production in cells (Fig. 1N and fig. S3W), which were correlated with increased migration of MDA-MB-231 cells in vitro (Fig. 1, O and P) regardless of STING (fig. S3, X and Y).

Other than STING, the other known 2′3′-cGAMP binding partner is EF1A1, where 2′3′-cGAMP binds and suppresses EF1A1 guanosine triphosphatase (GTPase) activity (*29*). Depletion of EF1A1 by sgRNAs (fig. S3Z) did not affect 2′3′-cGAMP–induced migration of MDA-MB-231 cells (fig. S3, z1 and z2). These data suggest that 2′3′-cGAMP is unlikely to promote cell migration through EF1A1.

2′3′-cGAMP interactome identifies the GTPase Rab18 as a binding partner

To find the potential 2′3′-cGAMP effector(s) involved in cell migration control other than STING and EF1A1, we performed a biotin-2′3′-cGAMP pull-down–coupled proteomic analysis (Fig. 2A). We chose c[G(2′,5′)p-2′-Biotin-16-A(3′,5′)p] as the probe largely because structural analysis of 2′3′-cGAMP binding to STING shows that both GMP and AMP moieties are involved in STING interactions [Protein Data Bank (PDB): 4LOH]. We validated c[G(2′,5′)p-2′-Biotin-16-A(3′,5′)p] as a suitable bait as it could pull down endogenous STING from THP1 cell lysates and label-free 2′3′-cGAMP competed with c[G(2′,5′)p-2′-Biotin-16-A(3′,5′)p] to bind STING (fig. S4A). We chose THP1 monocytes largely because they are commonly used for cGAS/cGAMP/STING signaling studies with an intact DNA sensing pathway where STING is served as a suitable positive control. c[G(2′,5′)p-2′-Biotin-16-A(3′,5′)p] pull-downs from THP1 monocytes showed enrichment of unknown proteins (fig. S4B), and mass spectrometry analysis identified 225 unknown 2′3′-cGAMP binding partners with a $\log_2$ fold change value larger than 1.5. Pathway analysis of the 225 binging partners by metascape.org showed an enrichment for pathways involving neutrophil degranulation, regulation of GTPase activity, and others (fig. S4, C and D). Considering that GTPases such as Rho and Rac have been tightly connected with cell motility control (*30*), the group of GTPases/guanine nucleotide exchange factors (GEFs)/GTPase activating proteins (GAPs) drew our attention (Fig. 2C). We hypothesized that 2′3′-cGAMP might regulate certain GTPase(s) to promote cell migration. We recognize that this approach does not rank candidates based on cGAMP binding affinity and is affected by stoichiometry and cellular localization of each protein. Thus, it provides a reference for us to further select true cGAMP binding proteins.

To determine the identity(ies) of the potential 2′3′-cGAMP binding GTPase(s) facilitating cell migration, we depleted most of the GTPases, GEFs, and GAPs from the proteomic analysis (Fig. 2C) by two to three independent shRNAs. In particular, we found that depletion of the GTPase Rab18 consistently suppressed MDA-MB-231 cell migration triggered by 2′3′-cGAMP in vitro by all three shRNAs (Fig. 2, D and E). Although depletion of GAPVD1, GDI2, or ARHGE2 also reduced 2′3′-cGAMP–induced cell migration, we did not focus on these targets since migration suppression caused by Rab18 depletion was more marked. Notably, Rab18 depletion (Fig. 2F) did not reduce MDA-MB-231 cell growth (fig. S4, E and F) but attenuated 2′3′-cGAMP–induced cell migration (Fig. 2, G and H, and fig. S4, G and H). Supporting a STING-independent 2′3′-cGAMP function in promoting cell migration, depletion of STING did not notably reduce 2′3′-cGAMP–triggered MDA-MB-231 cell migration, while additional depletion of Rab18 reduced 2′3′-cGAMP–induced cell migration (Fig. 2, I to K). Notably, Rab18 depletion did not notably affect MDA-MB-231 cell migration driven by 10% FBS (fig. S4, I and J), supporting a specificity for Rab18 in mediating 2′3′-cGAMP–triggered cell migration. Together, these data suggest that Rab18 mediates 2′3′-cGAMP–controlled cell migratory ability.

Characterization of 2′3′-cGAMP binding to Rab18

Next, we characterized how 2′3′-cGAMP binds and regulates Rab18. We found that biotin-2′3′-cGAMP interacted with bacterially purified glutathione *S*-transferase (GST)–Rab18 recombinant proteins (Fig. 3A) with a dissociation constant (K_d) of ~0.3 mM (fig. S5, A and B), and GST-tag removed Rab18 proteins in vitro (Fig. 3B), supporting a direct binding between 2′3′-cGAMP and Rab18. Furthermore, endogenous Rab18 immunoprecipitated endogenous 2′3′-cGAMP in MDA-MB-231 cells (Fig. 3C) like STING (fig. S5C). We also observed that biotin-2′3′-cGAMP pulled down endogenous Rab18 or STING proteins from either MDA-MB-231 cells (Fig. 3D) or MEFs (fig. S5D). Moreover, biotin-cAMP failed to pull down GST-Rab18 proteins where biotin-cGAMP could (fig. S5E). In addition, biotin-2′3′-cGAMP specifically pulled down endogenous Rab18 but not its close small GTPase family members Rab27A or Rab3 (fig. S5F). To determine the critical residues in Rab18 mediating 2′3′-cGAMP binding, using various bioinformatic tools including Prankweb based on a solved crystal structure of Rab18 binding to Gppnhp [nondegradable guanosine triphosphate (GTP)] (PDB: 1x3s), we generated a simulated structure of Rab18 binding to 2′3′-cGAMP (Fig. 3E and fig. S5G). This led to identification of two potential 2′3′-cGAMP binding pockets including pocket 1 partially overlapped with GTP binding motif (fig. S5H) and an uncharacterized pocket 2 (fig. S5I). A pocket 3 was selected as a negative control with a calculated binding energy of −30.8 kCal/mol (fig. S5J). Given that the binding energy in pocket 1 (−44.6 kCal/mol) and pocket 2 (−42.2 kCal/mol) are similar and are both much lower than in pocket 3 (the negative control), this indicates that cGAMP may bind either pocket 1 or pocket 2. 2′3′-cGAMP binding to pocket 1 would compete with GTP loading to Rab18; thus, we next examined whether 2′3′-cGAMP binding to Rab18 suppresses Rab18 GTPase activity in vitro. We purified GST-Rab18 recombinant proteins from bacteria (fig. S5K) and found that these Rab18 proteins were loaded with low amounts of GTP/guanosine diphosphate (fig. S5L). GST-Rab18 proteins could pull down endogenous 2′3′-cGAMP but not 3′3′-cGAMP from MDA-MB-231 cells (fig. S5M). GTP addition could further activate Rab18 in an in vitro GTPase assay (Fig. 3F). Furthermore, we observed that 2′3′-cGAMP alone failed to activate Rab18 GTPase, but 2′3′-cGAMP further facilitated GTP-induced Rab18 activation at either lower (Fig. 3G) or higher GTP concentrations (Fig. 3H). Moreover, GTP addition did not notably affect biotin-2′3′-cGAMP binding to GST-Rab18 recombinant proteins in vitro (Fig. 3I), suggesting that GTP binding does not affect 2′3′-cGAMP binding to Rab18. In echoing these findings, 2′3′-cGAMP exerted a synergy with GTP in promoting MDA-MB-231 cell migration (fig. S5, N and O). Together, these data suggest that 2′3′-cGAMP does not compete with GTP for Rab18 binding, rather 2′3′-cGAMP synergizes with GTP to activate Rab18. This is further supported by identifying the allosteric pathways between these two binding pockets (Fig. 3J and fig. S5P) using Ohm (https://dokhlab.med.psu.edu/ohm), a previously developed algorithm to analyze allosteric communication networks within proteins

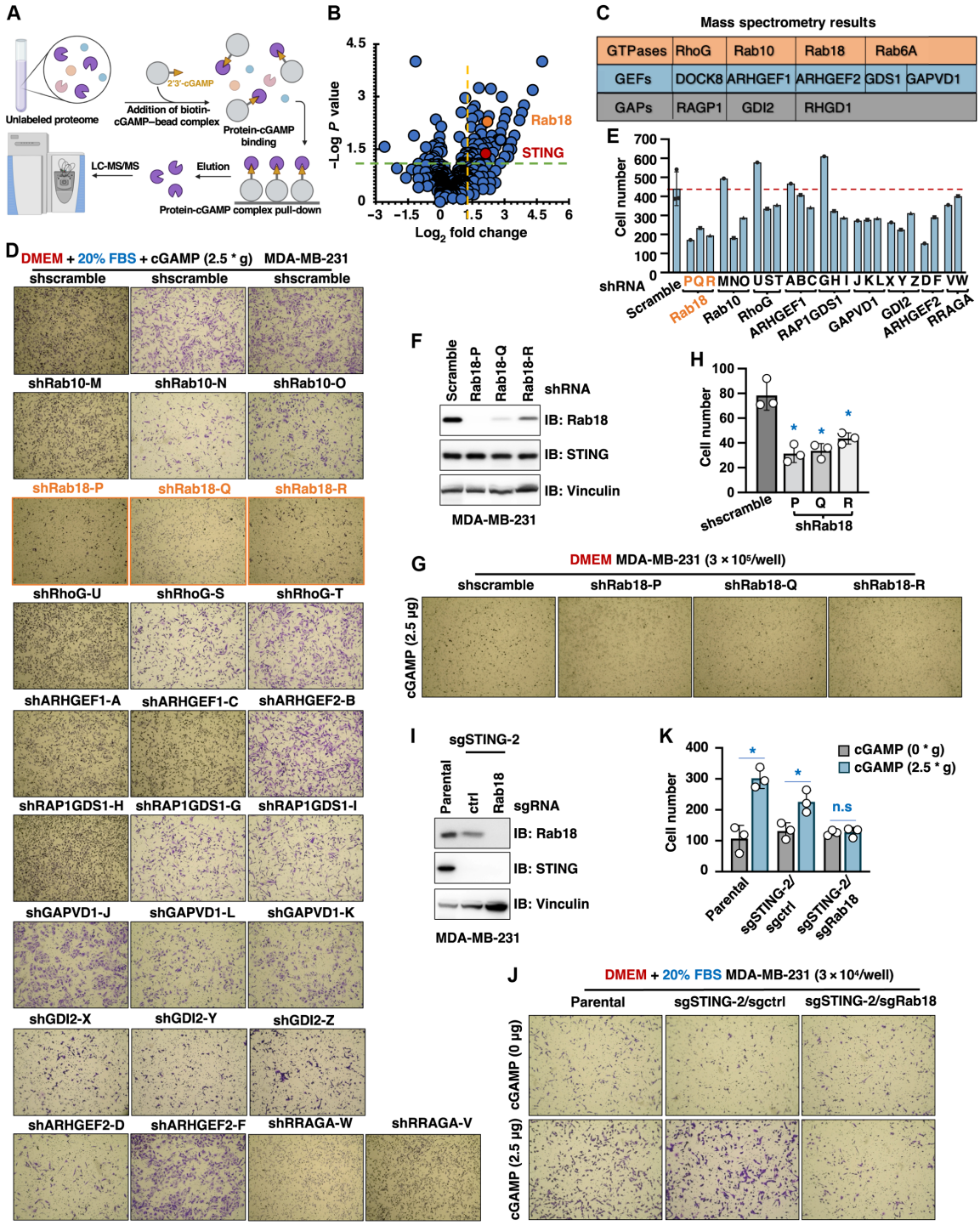

Fig. 2. 2′3′-cGAMP binds Rab18 to promote cell migration. (**A**) A cartoon illustration of the pipeline for the chemical-proteomic approaches to identify 2′3′-cGAMP binding partners. This model image is generated using BioRender. (**B**) A volcano plot from (A) showing significantly enriched (log_2 fold change equals or larger than 1.5) 2′3′-cGAMP binding proteins. (**C**) A list of GTPases, GEFs, and GAPs from (B). (**D** and **E**) Representative images of transwell assays using 3×10^4 indicated MDA-MB-231 cells under indicated conditions for 24 hours. Where indicated, MDA-MB-231 cells were infected with indicated shRNA viruses and selected in puromycin (1romyci to eliminate noninfected cells for 72 hours before cell collection. Transwell assays data are quantified in (E). Where indicated, 2.5 g of 2′3′-cGAMP is used in 300 liters of serum-free media in transwells. (**F**) IB analysis of WCL derived from indicated MDA-MB-231 cells. (**G** and **H**) Representative images of transwell assays using 3×10^5 indicated MDA-MB-231 cells treated with 2.5 g of 2′3′-cGAMP (in 300 liters of serum-free media in transwells) for 24 hours. Error bars were calculated as mean ± SD, $n = 3$ biological replicates. *$P < 0.05$ (one-way ANOVA test). (**I**) IB analysis of WCL derived from indicated MDA-MB-231 cells. (**J** and **K**) Representative images of transwell assays using 3×10^4 indicated MDA-MB-231 cells under indicated conditions for 24 hours and quantified in (K). Error bars were calculated as mean ± SD, $n = 3$ biological replicates. *$P < 0.05$ (one-way ANOVA test). Where indicated, 2.5 g of 2′3′-cGAMP is used in 300 liters of serum-free media in transwells.

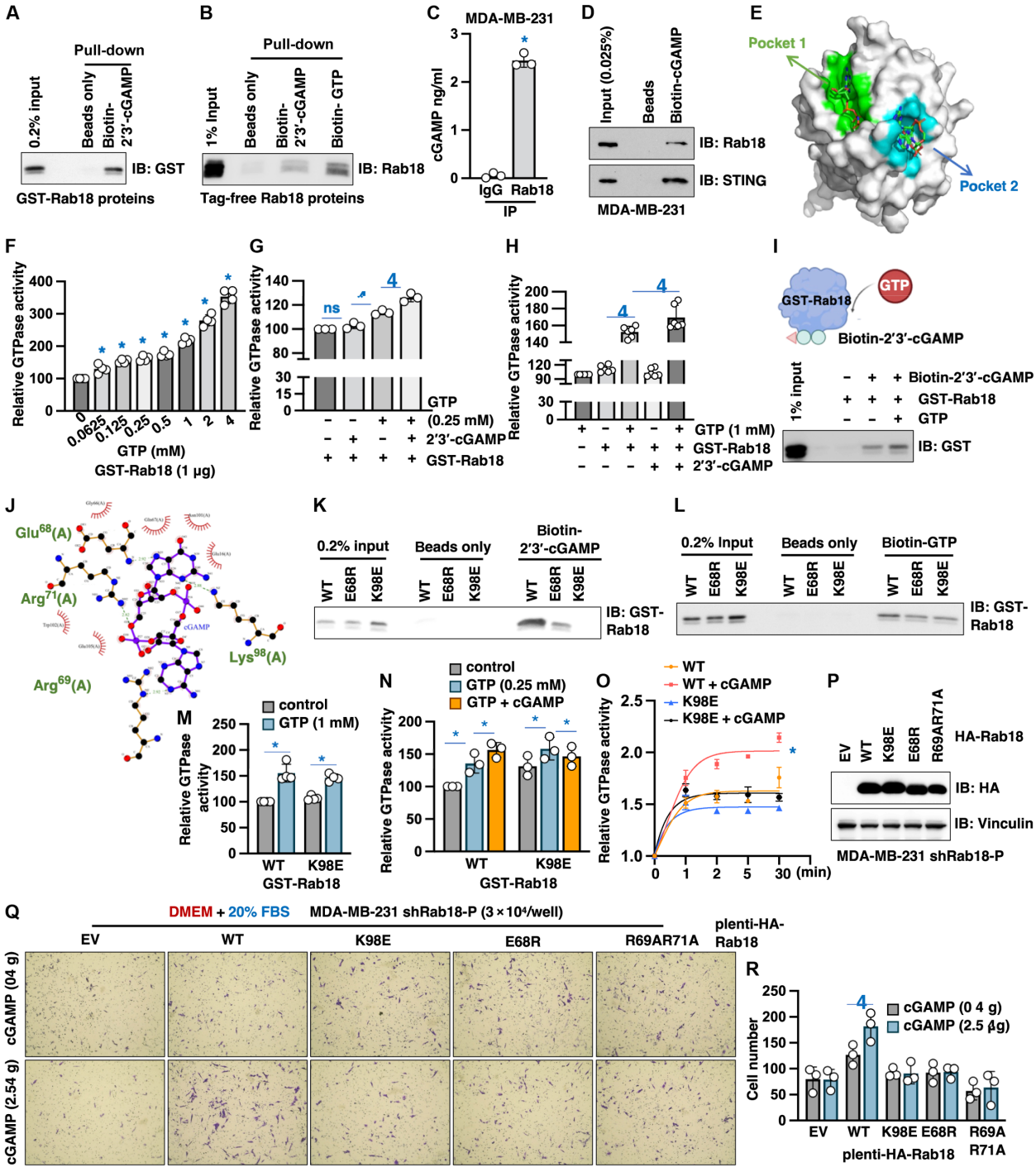

Fig. 3. 2′3′-cGAMP binds Rab18-E68, R69, R71, and K98 residues to facilitate Rab18 activation. (**A** and **B**) Immunoblot (IB) analysis of biotin-2′3′-cGAMP and biotin-GTP pull-downs using bacterially purified GST-Rab18 (A) or tag-free Rab18 (B) proteins. (**C**) 2′3′-cGAMP ELISA analysis of endogenous Rab18-IPs (immunoprecipitations) using MDA-MB-231 lysates. (**D**) IB analysis of biotin-2′3′-cGAMP pull-downs from MDA-MB-231 whole cell lysates (WCL). (**E**) An illustration of a simulated 2′3′-cGAMP/Rab18 complex structure by MedusaDock, and interacting Rab18 residues were identified by Prankweb. (**F** to **H**, **M**, and **N**) In vitro Rab18 GTPases activity assays using bacterially purified GST-Rab18 proteins under indicated conditions. Error bars were calculated as mean ± SD, $n = 6$ biological replicates. *$P < 0.05$ (one-way ANOVA test). (**I**) IB analysis of biotin-2′3′-cGAMP pull-downs using GST-Rab18 proteins with GTP. The cartoon illustration is generated using BioRender. (**J**) An illustration of Rab18 residues interacting with 2′3′-cGAMP from the structural simulation by Prankweb. (**K** and **L**) IB analyses of biotin-2′3′-cGAMP (K) or biotin-GTP (L) pull-downs using indicated GST-Rab18 proteins. (**O**) In vitro Rab18 GTPases activity assays by incubating indicated GST-Rab18 proteins with or without 2′3′-cGAMP for indicated periods. (**P**) IB analysis of WCL derived from indicated MDA-MB-231 cells. EV, empty vector control. (**Q** and **R**) Representative images of transwell assays using indicated numbers of indicated MDA-MB-231 cells under indicated conditions for 24 hours. Error bars were calculated as mean ± SD, $n = 3$ biological replicates. *$P < 0.05$ (one-way ANOVA test). Where indicated, 2.5 μg of 2′3′-cGAMP is used in 300 liters of serum-free media in transwells.

aimed to identify critical coupled residues for experimental testing or drug development (*31*).

Next, we tested whether pocket 2 mutations (Fig. 3J; including K98, E68, R69, and R71) impair Rab18 binding to 2′3′-cGAMP and attenuate 2′3′-cGAMP–aided Rab18 activation. We first purified GST-Rab18-K98E and E68R recombinant proteins (fig. S6A). Compared with GST-Rab18-WT proteins, Rab18-E68R and, to a higher extent, K98E proteins were deficient in binding biotin-2′3′-cGAMP in vitro (Fig. 3K). On the other hand, these two mutants showed a comparable binding affinity with biotin-GTP under the same experiment conditions (Fig. 3L). These data support the notion that both E68 and K98 residues may be directly involved in 2′3′-cGAMP binding. Given that the K98E mutant displays a more severe deficiency in binding biotin-cGAMP, we will focus on this mutant in the remainder of the study to dissect effects of Rab18 deficiency in binding 2′3′-cGAMP but not GTP. Consistent with this finding, we observed that in in vitro GTPase assays, GTP induced comparable activation of both GST-Rab18-WT and GST-Rab18-E98K proteins (Fig. 3M); however, unlike GST-Rab18-WT, 2′3′-cGAMP failed to further induce GST-Rab18-E98K activation (Fig. 3, N and O, and fig. S6B). We further reexpressed WT- and various 2′3′-cGAMP binding–deficient Rab18-K98E or E68R mutants in Rab18-depleted MDA-MB-231 cells (Fig. 3P) and found that 2′3′-cGAMP triggered migration of MDA-MB-231 cells expressing WT-Rab18 but not K98E nor E68R-Rab18 (Fig. 3, Q and R). On the other hand, unlike GST-Rab18-WT, GTP addition failed to activate GST-Rab18-S17A (pocket 1 mutation deficient in binding GTP) GTPases in vitro (fig. S6, C and D). As a result, expressing the Rab18-S17A mutant in endogenous Rab18-depleted MDA-MB-231 cells (fig. S6E) failed to respond to 2′3′-cGAMP–induced cell migration (fig. S6F). This was largely due to that Rab18-S17A mutant although bound 2′3′-cGAMP, it was deficient in GTP binding (fig. S6G). Together, these data support the notion that 2′3′-cGAMP promotes MDA-MB-231 cell migration largely through binding Rab18 pocket 2 including K98 and E68 residues. Notably, expressing 2′3′-cGAMP binding–deficient K98E- or E68R-Rab18 mutants did not notably affect unstimulated cell growth (fig. S6, H and I), cellular distribution of Rab18 (fig. S6J), or lipid droplet formation by Rab18 in cells (fig. S6K), excluding the possibility that attenuated cell migration observed in Rab18 mutants deficient in binding 2′3′-cGAMP is caused by deregulated Rab18 function in growth or lipid droplet formation.

In addition, we also similarly simulated 3′2′-cGAMP or 3′3′-cGAMP binding to Rab18 (fig. S6, L to N). Unlike 2′3′-cGAMP, the outward-facing guanine in 3′2′-cGAMP did not interact with R69, and both adenine and guanine were facing inward in 3′3′-cGAMP, lacking interactions with R69 (fig. S6, M to O). Thus, in both Rab18 pockets 1 and 2, 2′3′-cGAMP exerted the highest binding affinity (evidenced by the lowest binding energy) compared to 3′2′-cGAMP or 3′3′-cGAMP (fig. S6P). These data provide further mechanistic insights for the specificity of 2′3′-cGAMP but not other linkages of cGAMP in binding and regulating Rab18.

RNA-seq analysis identifies FosB as a downstream effector mediating 2′3′-cGAMP/Rab18 signaling in cell migration control

We next examined downstream effectors mediating 2′3′-cGAMP/Rab18 signaling that promote cell migration. Rab18 has been reported to regulate focal adhesion dynamics by chemotaxis in U2OS cells (*32*). We found that in MDA-MB-231 cells, 2′3′-cGAMP treatment did not affect FAK-pY397 signals (fig. S7A) nor regulated focal adhesion dynamics (fig. S7B), suggesting that reported Rab18 regulation on focal adhesion may not be a major signaling through which 2′3′-cGAMP/Rab18 promotes MDA-MB-231 cell migration. Notably, we pretreated MDA-MB-231 cells with 2′3′-cGAMP and observed a robust effect in inducing cell migration (fig. S7, C to F). Thus, we thought that 2′3′-cGAMP–induced Rab18 activation may function through regulating certain transcriptional programs to control cell migration. RNA sequencing (RNA-seq) analyses of THP1$^{STING-/-}$ monocytes treated with 2′3′-cGAMP compared to untreated control yielded only 13 genes with statistically significant changes (11 up and 2 down; table S1). Notably, unlike 2′3′-cGAMP, neither 3′3′-cGAMP nor 3′2′-cGAMP could promote expression of these genes (fig. S7G). Among these 11 up-regulated genes, NAB2 (*33*), FosB (*34*), C3AR1 (*35*), and LIMA1 (*36*) have been associated with cell migration (Fig. 4A). We thus examined mRNA changes of these targets in MDA-MB-231 cells upon 2′3′-cGAMP stimulation by quantitative reverse transcription polymerase chain reaction (qRT-PCR) and observed that 2′3′-cGAMP substantially increased mRNA levels of FosB and, to a lesser extent, C3AR1 (Fig. 4B). Furthermore, we performed RT^2 Profiler PCR arrays in MDA-MB-231-shSTING (STING-depleted) cells treated with or without 2′3′-cGAMP and found that 2′3′-cGAMP addition also increased FosB mRNA expression (Fig. 4C). Treatment of MDA-MB-231 cells with 2′3′-cGAMP induced FosB protein expression but not other characterized migration promoting proteins such as SLUG, Moesin, melanocyte inducing transcription factor (MITF), or E-cadherin (Fig. 4D). Increased FosB expression by 2′3′-cGAMP stimulation was also observed in MDA-MB-231-sgSTING (fig. S7H), MEFs (fig. S7I), and STING-depleted MEFs (fig. S7J) to promote cell migration (fig. S7, K and L). Unlike 2′3′-cGAMP, adenosine addition did not induce FosB expression (fig. S7M), nor inhibiting adenosine receptor A2B by MRS-1706 affected FosB expression (fig. S7N). Moreover, 2′3′-cGAMP–induced FosB expression depended on Rab18 (Fig. 4E and fig. S7O). Compared with WT-Rab18 expressing MDA-MB-231 cells, 2′3′-cGAMP failed to induce FosB2 expression in K98E or E68R-Rab18 expressing cells (Fig. 4F). These data suggest that 2′3′-cGAMP/Rab18 signaling may induce FosB expression in cell migration control. Furthermore, depletion of endogenous FosB in MDA-MB-231 cells (Fig. 4G) reduced cell migration triggered by 2′3′-cGAMP (Fig. 4, H and I). Notably, FosB2 is the major isoform expressed in MDA-MB-231 cells, and reexpressing FosB2 in FosB-depleted cells (fig. S7P) largely rescued 2′3′-cGAMP–induced cell migration (fig. S7, Q and R). Thus, in this study, we focus on the FosB2 isoform. Notably, 2′3′-cGAMP treatment increased intracellular 2′3′-cGAMP levels within 0.5 hours (fig. S7S), induced FosB transcription within 1 hour (fig. S7T), and subsequently facilitated FosB protein expression at later time points (fig. S7U), revealing a signaling cascade (fig. S7V). Eventually, 2′3′-cGAMP treatment drove FosB nuclear enrichment (fig. S7W) to presumably facilitate its transcriptional function. In addition to breast cancer cells, 2′3′-cGAMP treatment also increased FosB expression in colon cancer DLD-1 cells (fig. S7X). Cumulatively, these data indicate that 2′3′-cGAMP/Rab18 signaling promotes cell migration largely through inducing FosB transcription.

Increasing endogenous 2′3′-cGAMP levels by low-dose Dox (fig. S3E) also increased FosB expression in MDA-MB-231 (Fig. 4J and fig. S7Y) and MCF-7 cells (fig. S7Z). Dox-induced FosB transcription (fig. S7z1) depended on cGAS (as Dox induces cGAS activation and thus 2′3′-cGAMP production; fig. S7z2) and Rab18 (Fig. 4K and fig. S7z3). Therefore, either loss of cGAS (fig. S7z4), depletion of Rab18 (Fig. 4L and fig. S7z5), expressing various Rab18 mutants deficient in binding 2′3′-cGAMP (Fig. 4, M and N), or depletion of

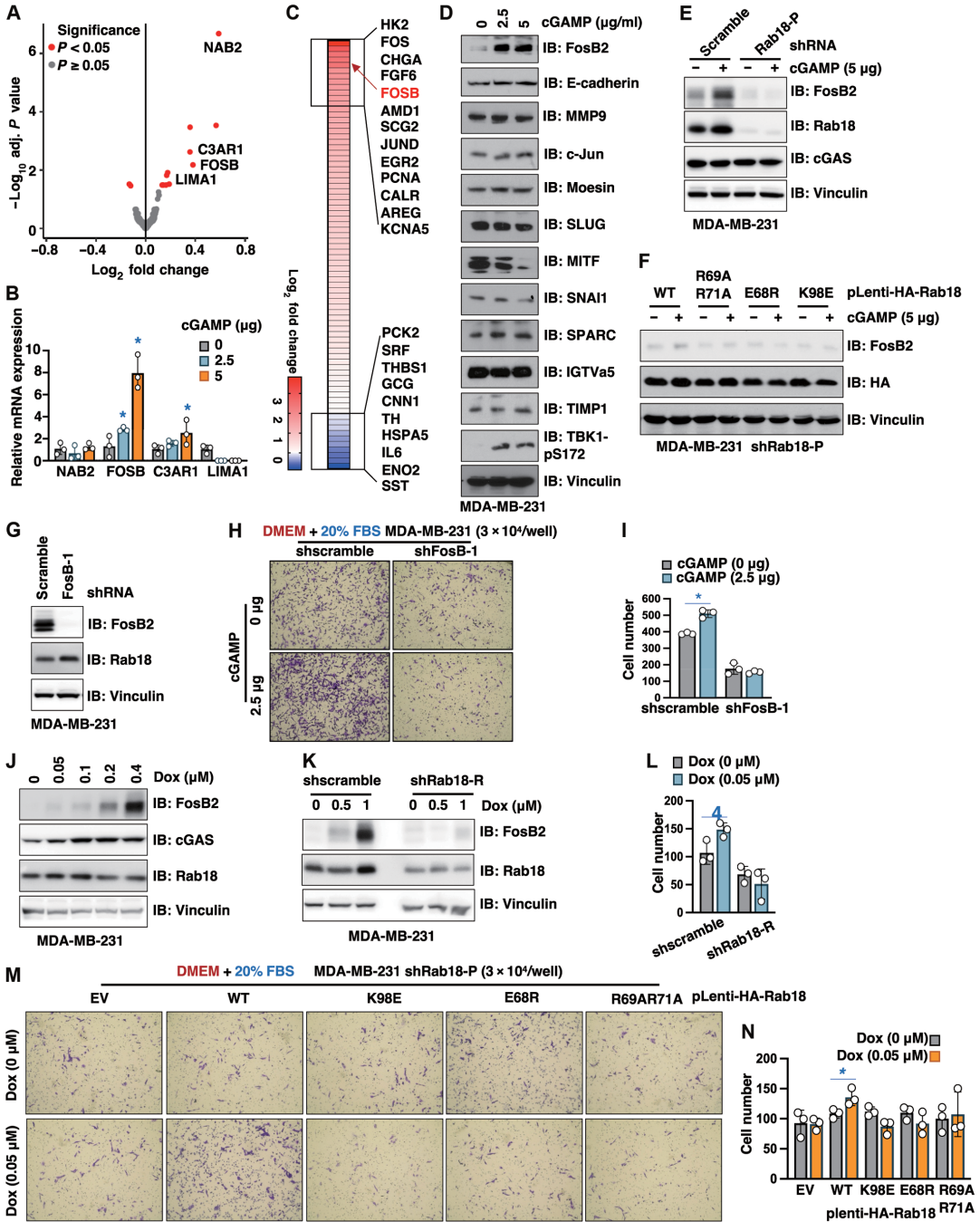

Fig. 4. 2′3′-cGAMP/Rab18 signaling promotes FosB transcription and expression to facilitate cell migration. (**A**) A volcano plot from RNA-seq data from THP1$^{STING-/-}$ cells comparing 2′3′-cGAMP–induced gene transcriptional changes in THP1-*STING*$^{-/-}$ cells. (**B**) RT-PCR analyses of expression changes of indicated genes from MDA-MB-231 cells treated with indicated of 2′3′-cGAMP (2.5MP edan for 2 hours. (**C**) A representative heatmap for genes with indicated changes using RT^2 Profiler PCR arrays by comparing MDA-MB-231-shSTING cells treated with 2′3′-cGAMP (2.5MP ays for 2 hours compared with vehicle treatment control cells. (**D**) IB analysis of WCL from MDA-MB-231 cells treated with indicated doses of 2′3′-cGAMP for 24 hours. (**E** and **F**) IB analysis of WCL from indicated MDA-MB-231 cells treated with indicated doses of 2′3′-cGAMP for 24 hours. (**G**) IB analysis of WCL from indicated MDA-MB-231 cells. Where indicated, MDA-MB-231 cells were infected with indicated shRNA viruses and selected in puromycin (1romyci to eliminate noninfected cells for 72 hours before cell collection. (**H** and **I**) Representative images of transwell assays using 3 × 10^4 control or FosB-depleted MDA-MB-231 cells treated with indicated doses of 2′3′-cGAMP for 24 hours. Error bars were calculated as mean ± SD, $n = 3$ biological replicates. *$P < 0.05$ (one-way ANOVA test). Where indicated, 2.5 g of 2′3′-cGAMP is used in 300 liters of serum-free media in transwells. (**J** and **K**) IB analysis of WCL derived from indicated MDA-MB-231 cells treated with indicated doses of Dox for 24 hours before cell collection. (**L**) Quantifications of transwell assays using indicated numbers of control or FosB-depleted MDA-MB-231 cells treated with indicated doses of Dox for 24 hours. Error bars were calculated as mean ± SD, $n = 3$ biological replicates. *$P < 0.05$ (one-way ANOVA test). (**M** and **N**) Representative images of transwell assays using indicated cells under indicated conditions for 24 hours (M) and quantified in (N). Error bars were calculated as mean ± SD, $n = 3$ biological replicates. *$P < 0.05$ (one-way ANOVA test).

FosB (fig. S7, z6 and z7) led to attenuation of Dox-induced MDA-MB-231 cell migration.

Intratumor bacterium *S. aureus* infection induces 2′3′-cGAMP synthesis in cells to facilitate cell migration

Recently, intratumor bacteria were identified and characterized (*37*) to promote metastatic colonization (*38*). Considering intracellular microbiome triggers cGAS activation to induce synthesis of endogenous 2′3′-cGAMP (*39*), we thought to investigate whether intratumor bacterial infection facilitates cell migration through the 2′3′-cGAMP/Rab18/FosB signaling. To this end, we chose *Staphylococcus aureus*, a human pathogenic bacterial species found in human breast tumors (*37*). Coculture of *S. aureus* with MDA-MB-231 cells in vitro led to intracellular retention of *S. aureus* (fig. S8A). This induced cGAS/STING pathway activation as evidenced by increased IRF3-pS396 and STING-pS366 signals (Fig. 5A), largely through promoting 2′3′-cGAMP synthesis in cells (Fig. 5B and fig. S8B). Incubating MDA-MB-231 cells with *S. aureus* substantially increased cell migration ability (Fig. 5, C and D, and fig. S8C). To further eliminate effects of extracellular *S. aureus* in this assay, gentamycin and ampicillin alone or in combination were used to specifically remove extracellular but not intracellular *S. aureus* in this coculture model. Consistent with a previous report (*38*), either treatment efficiently removed extracellular *S. aureus* (Fig. 5E) but retained the ability of cytosolic *S. aureus* in triggering cGAS activation evidenced by increased IRF3-pS396 signals presumably through 2′3′-cGAMP synthesis (Fig. 5F). In addition, we found that *S. aureus* infection promoted control but not cGAS-deleted MDA-MB-231 cell migration (fig. S8, D and E), as well as STING depletion did not affect *S. aureus* infection–induced cell migration (fig. S8, F and G), further supporting the dependence of *S. aureus* infection on cGAS/2′3′-cGAMP signaling in cell migration control. We observed that depletion of either Rab18 (Fig. 5, G and H) or FosB (Fig. 5, I and J) largely abolished *S. aureus* infection–induced MDA-MB-231 cell migration. This is consistent with our observation that intracellular *S. aureus* infection induced FosB expression in a Rab18-dependent manner (Fig. 5K) to facilitate cell migration. Moreover, in a tail vein injection murine model, we confirmed that *S. aureus*–infected MDA-MB-231 cells exerted enhanced migratory ability to mouse lungs, and depletion of Rab18 attenuated this effect (Fig. 6, A to C, and fig. S8, G and I). No significant mouse body weight differences were observed among these groups (fig. S8J), and no sign of *S. aureus* infection was observed (such as reported eye and skin infection). Together, these data suggest that breast tumor residing bacterium *S. aureus* may facilitate breast cancer metastasis partially through activating our identified 2′3′-cGAMP/Rab18/FosB signaling.

HSV-1 infection–induced 2′3′-cGAMP production facilitates cell migration

Given that the canonical cGAS function is to serve as a cytosolic DNA sensor to activate innate immunity in responding to DNA viral infection by synthesizing 2′3′-cGAMP, to further investigate whether DNA viral infection induced 2′3′-cGAMP facilitates cell migration, we collected supernatants from herpes simplex virus 1 (HSV-1)–infected MDA-MB-231 cells that presumably containing 2′3′-cGAMP and found that these supernatants induced MDA-MB-231 cell migration (Fig. 6D). To further reveal whether HSV-1 infection–induced 2′3′-cGAMP plays a role in this process, before HSV-1 infection, we treated MDA-MB-231 cells with cGAS inhibitor G140 and found that supernatants from these cGAS-inhibited cells were deficient in driving cell migration compared with control supernatants (Fig. 6, E and F). These data suggest that upon DNA viral infection conditions, tumor cell synthesized that 2′3′-cGAMP might be able to drive tumor metastasis; however, further in-depth investigations are warranted to use animal models to examine this hypothesis more rigorously.

Rab18 deprenylation by statins inhibits 2′3′-cGAMP recognition and cell migration

In addition to chemotherapeutic agents like Dox that trigger DNA damage and 2′3′-cGAMP production, other agents such as lovastatin were also reported to induce 2′3′-cGAMP production and STING activation in colon cancer in a small heterodimer partner 2–dependent manner (*40*). In MDA-MB-231 cells, unlike in colon cancer (*40*), treatment with lovastatin did not notably induce DNA damage (fig. S9A) but rather caused a marked Rab18 mobility shift in SDS–polyacrylamide gel electrophoresis (SDS-PAGE) in a lovastatin dose–dependent (Fig. 7A and fig. S9B) but cGAS-independent manner (fig. S9, C and D). Other statins such as atorvastatin also induced a Rab18 mobility shift in MDA-MB-231 cells (fig. S9E). We speculated that this Rab18 protein mobility shift was due to post-translational modifications. Considering other small GTPases such Ras has been reported to undergo prenylation leading to a faster mobility shift in SDS-PAGE (*41*), we hypothesized that statins might suppress Rab18 prenylation. Given that prenylation largely occurs on a C-terminal CAAX motifs (*42*) and Rab18 contains such a motif (Fig. 6B), we next mutated Rab18-C203 residue to Ala and observed that not only the C203A-Rab18 mutant displayed a retarded mobility in SDS-PAGE but also, unlike WT-Rab18, lovastatin failed to trigger cell mobility changes (Fig. 7B). Biotin-2′3′-cGAMP could pull down endogenous prenylated Rab18 from MDA-MB-231 cells but failed to interact with lovastatin-triggered de-prenylated forms of Rab18 (Fig. 7C). These data suggest that lovastatin-mediated Rab18 deprenylation may disrupt 2′3′-cGAMP binding. Lovastatin inhibited MDA-MB-231 cell migration driven by either FBS (fig. S9, F to I), 2′3′-cGAMP (Fig. 7, D and E), or Dox (fig. S9, J and K), presumably through blocking the cGAMP/Rab18 interactions (fig. S9L). Furthermore, restoring Rab18-C203A expression in endogenous Rab18-depleted MDA-MB-231 cells (Fig. 7F) failed to respond to 2′3′-cGAMP–induced cell migration (Fig. 7, G and H) that presumably due to inability for this mutant to increase FosB2 expression upon 2′3′-cGAMP treatment (fig. S9M). Together, this demonstrates that lovastatin-induced Rab18 deprenylation at C203 abolishes Rab18 binding to 2′3′-cGAMP, therefore attenuating 2′3′-cGAMP-induced cell migration. Notably, pretreatment with low doses of Dox also increased migratory ability of MDA-MB-231 cells (fig. S9, N and O), suggesting that cGAMP/Rab18/FosB-mediated transcriptional changes exert sustained effects in cell migration control. Consistent with a role of endogenous 2′3′-cGAMP in promoting cell migration through activating FosB-mediated transcriptional programs, in a tail vein injection murine model (fig. S9P), MDA-MB-231 cells pretreated either with the cGAS inhibitor G140 or lovastatin/Dox (Fig. 7I) or lovastatin alone (Fig. 7, J and K) to reduce endogenous 2′3′-cGAMP levels showed compromised cell migratory ability to lungs in NOD scid gamma (NSG) mice compared with control treatment, with no effects on animal body weights (Fig. 7L and fig. S9Q). In addition, lovastatin-induced Rab18 deprenylation in suppressing 2′3′-cGAMP–induced cell migration was also confirmed in colon cancer DLD-1 cells (fig. S9, R to T).

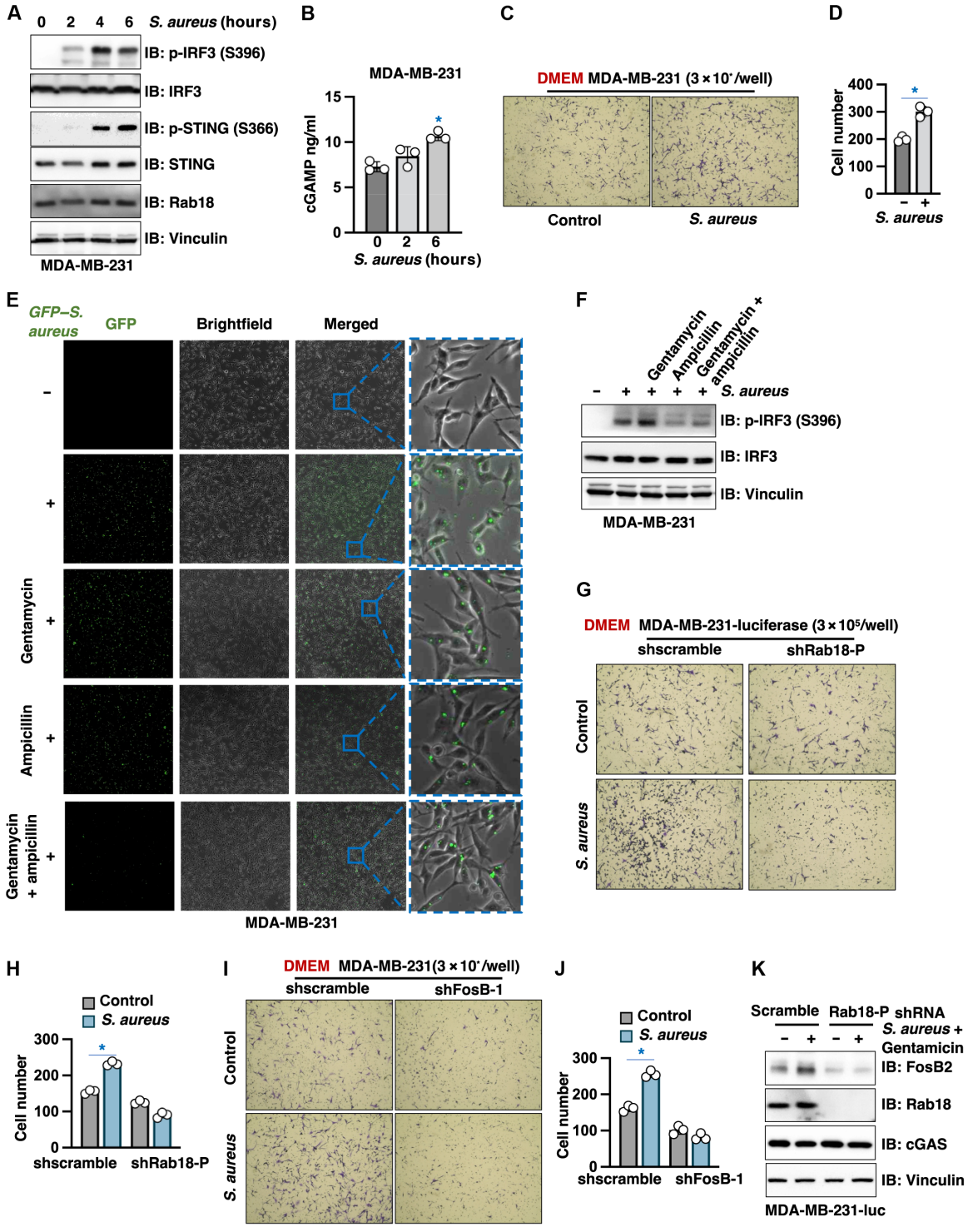

Fig. 5. *S. aureus* infection induces 2′3′-cGAMP synthesis in cells to promote MDA-MB-231 cell migration. (**A**) IB analysis of WCL derived from MDA-MB-231 cells infected with HG003 MSSA *S. aureus* for indicated time periods. (**B**) 2′3′-cGAMP ELISA quantifications of intracellular 2′3′-cGAMP levels in 10^6 MDA-MB-231 cells obtained from (A). (**C** and **D**) Representative images of transwell assays using 3×10^5 MDA-MB-231 cells infected with control or *S. aureus* for 6 hours followed by transwell assays and quantified in (D). Error bars were calculated as mean ± SD, $n = 3$ biological replicates. *$P < 0.05$ (one-way ANOVA test). (**E**) Representative immunofluorescent images of MDA-MB-231 cells infected with BC47 LAC-GFP *S. aureus* for 6 hours followed by treatment with indicated antibiotics for 1 hour. Concentrations of antibiotics are as below: gentamicin, 200 μg/ml; ampicillin, 200 μg/ml; doxycycline, 20 g/ml. (**F**) IB analysis of WCL from MDA-MB-231 cells obtained from (E). (**G** to **J**) Representative images of transwell assays using 3×10^5 indicated MDA-MB-231 cells infected with control or *S. aureus* for 6 hours in DMEM media and quantified in (H) and (J). Error bars were calculated as mean ± SD, $n = 3$ biological replicates. *$P < 0.05$ (one-way ANOVA test). (**K**) IB analysis of WCL from MDA-MB-231 cells obtained from (G).

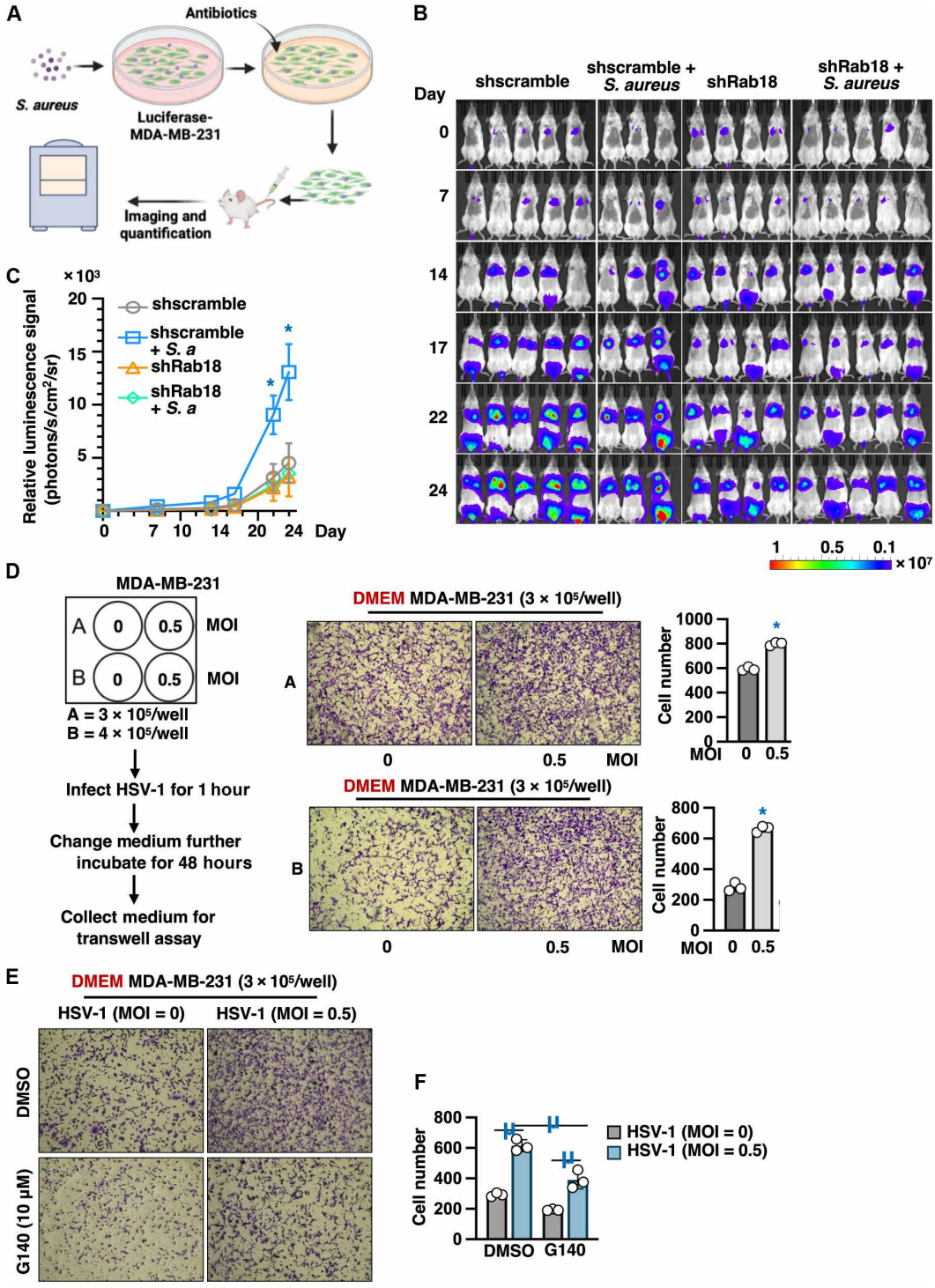

Fig. 6. *S. aureus* infection or HSV-1 infection induces MDA-MB-231 cell migration. (**A**) A cartoon illustration for the design of the NSG mouse tail vein injection assays. The cartoon illustration is generated using BioRender. (**B** and **C**) MDA-MB-231 cells stably expressing firefly luciferase were preinfected with vehicle or HG003 MSSA *S. aureus* (*S. a*) for 6 hours followed by treatment with gentamicin for 1 hour to remove noninfected bacteria. A total of 3×10^5 resulting cells were injected into tail veins of NSG mice, and noninvasive imaging was taken on indicated days postinjection (B) and quantified in (C). (**D**) Indicated number of MDA-MB-231 cells were infected with HSV-1 by indicated MOI, and supernatants were collected to perform transwell assays under indicated conditions and quantified. (**E**) Before HSV-1 infection, MDA-MB-231 cells were treated with G140 (10 mM) for 2 hours, and supernatants were similarly collected and used for transwell assays as in (D) and quantified in (**F**).

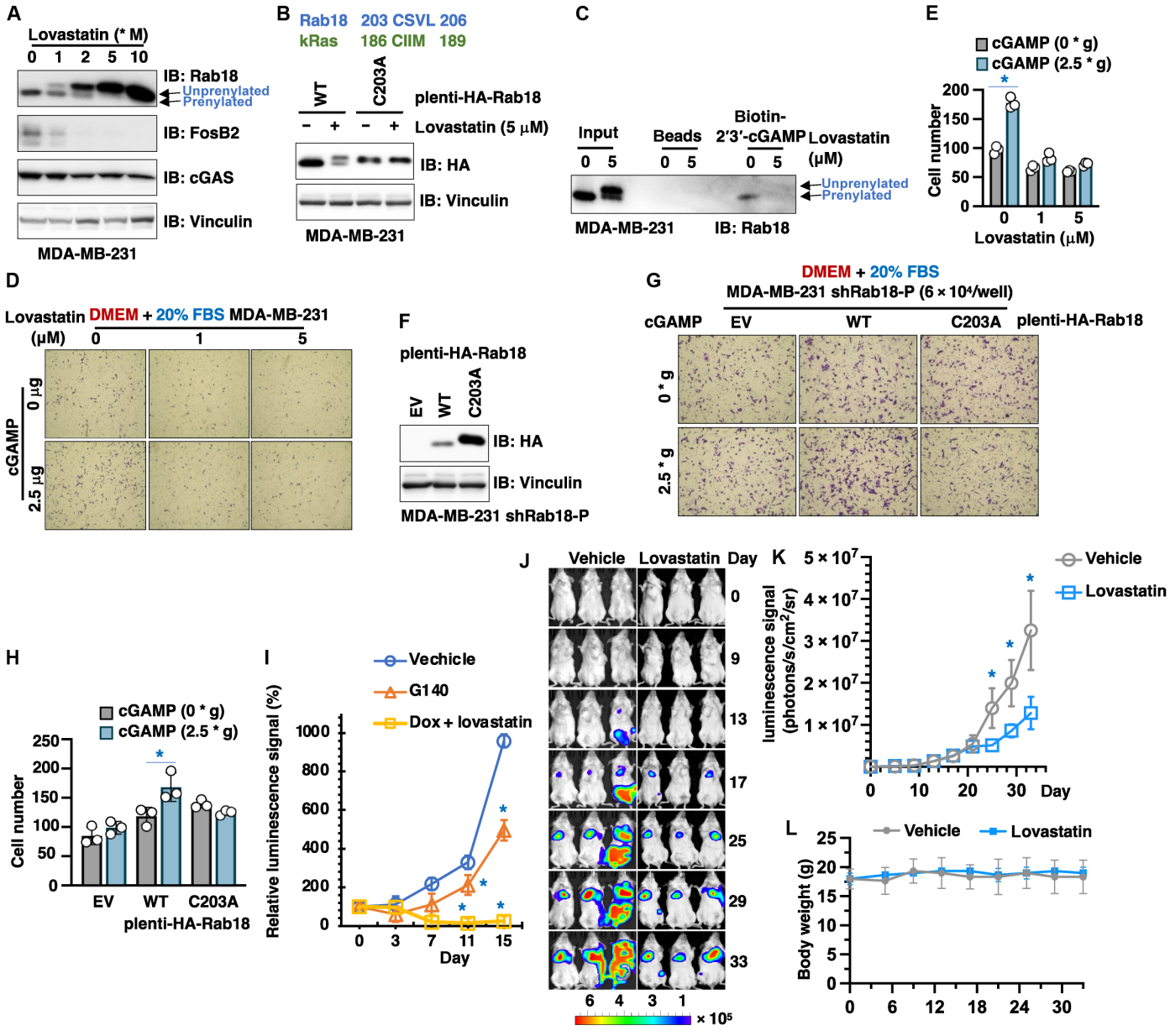

Fig. 7. Statin treatments induce Rab18 deprenylation to attenuate 2′3′-cGAMP binding. (**A**) IB analysis of WCL derived from MDA-MB-231 cells treated with indicated doses of lovastatin for 24 hours. Both prenylated and unprenylated species are labeled as indicated. (**B**) IB analysis of WCL derived from WT or C203A-Rab18 expressing MDA-MB-231 cells treated with 5 M lovastatin for 24 hours. (**C**) IB analysis of biotin-2′3′-cGAMP pull-downs from MDA-MB-231 cells treated with indicated doses of lovastatin for 24 hours. (**D** and **E**) Representative images of transwell assays using 3 × 10^4 MDA-MB-231 cells treated with indicated doses of 2′3′-cGAMP and lovastatin for 24 hours. Error bars were calculated as mean ± SD, $n = 3$ biological replicates. *$P < 0.05$ (one-way ANOVA test). (**F**) IB analysis of MDA-MB-231 cells stably expressing indicated Rab18 by lentiviral infection depleted of endogenous Rab18. (**G** and **H**) Representative images of transwell assays using 6 a 10^4 indicated MDA-MB-231 cells treated with indicated doses of 2′3′-cGAMP for 24 hours. Error bars were calculated as mean ± SD, $n = 3$ biological replicates. *$P < 0.05$ (one-way ANOVA test). (**I**) MDA-MB-231 cells stably expressing firefly luciferase were pretreated with vehicle, G140 (10 M), or Dox (0.05 M) with lovastatin (5 M) for 24 hours. A total of 5 × 10^5 resulting cells were injected into tail veins of NSG mice, and noninvasive imaging was performed on indicated days postinjection and quantified. (**J** to **L**) MDA-MB-231 cells stably expressing firefly luciferase were pretreated with vehicle or lovastatin (5 μM) for 24 hours. A total of 5 × 10^5 resulting cells were injected into tail veins of NSG mice, and noninvasive imaging was performed on indicated days postinjection (J) and quantified in (K). Animal body weights are shown in (L).

Together, these data suggest that lovastatin may suppress breast cancer metastasis in part through deprenylating Rab18 to inactivate the 2′3′-cGAMP/Rab18/FosB signaling.

DISCUSSION

Our study reveals a previously unidentified function of endogenous 2′3′-cGAMP in cell migration control beyond its previously characterized biological function including innate immune STING activation and suppression of EF1A1-mediated protein synthesis. By using a biotin-2′3′-cGAMP pull-down coupled proteomic approach, we establish the first 2′3′-cGAMP interactome in mammalian cells. Relying on this approach, we identify the small GTPase Rab18 as a previously unidentified and direct 2′3′-cGAMP binding partner and downstream effector, through binding and activation of which 2′3′-cGAMP promotes FosB transcription, leading to increased cell migration. This process is independent of previously characterized 2′3′-GAMP binding partners STING and EF1A1. Although Rab18 was not usually colocalized with STING in MDA-MB-231 cells (fig. S10A), STING depletion enhanced 2′3′-cGAMP interaction with Rab18 (fig. S10B) and vice versa (fig. S10C). These data suggest that, in cells, STING and Rab18 may compete for 2′3′-cGAMP binding (maybe due to stoichiometry or cellular localization of these molecules). In support of this notion, we observed that Rab18 depletion enhanced innate immune activation of MDA-MB-231 cells responding to ISD90 stimulation (fig. S10D), while reexpressing WT-Rab18 but not the 2′3′-cGAMP binding–deficient K98E-Rab18 in Rab18-depleted MDA-MB-231 cells suppressed innate immune activation (fig. S10E).

Furthermore, we demonstrate that distinct pathophysiological cues triggering accumulation of endogenous 2′3′-cGAMP promote cell migration in a 2′3′-cGAMP/Rab18/FosB signaling–dependent manner (fig. S10F). These distinct cues at least include low doses of chemotherapeutics such as Dox that induce DNA damage to cause accumulation of cytosolic DNA and infection by characterized intratumor bacteria such as *S. aureus*. Notably, how 2′3′-cGAMP–induced Rab18 activation facilitates FosB transcriptional activation and the major FosB transcriptional targets mediating cGAMP/Rab18-controlled cell migration remain elusive and warrant further in-depth investigations. Nonetheless, we observed increased FosB expression in MDA-MB-231 cells metastasis to lung (MDA-MB-4175) or bone (MDA-MB-1833) (fig. S10G), accompanied by increased migration ability (fig. S10, H and I). These correlative observations may suggest a role of 2′3′-cGAMP/FosB signaling in potentiating breast cancer metastasis. In addition, Rab18 has been reported to be overexpressed in multiple cancer types including gastric (*43*), liver (*44*), lung (*45*), and other cancers to promote cancer growth and metastasis, while loss of function of Rab18 mutants cause Warburg Micro syndrome (*46*). Similarly, FosB overexpression has also been reported in cancer to fuel tumorgenesis and treatment resistance (*47*). It is plausible that for cancers with high levels of Rab18, increased cellular 2′3′-cGAMP levels triggered by DNA damage, mitochondrial damage, or viral/bacterial infection are likely to function in activating Rab18 to promote tumor metastasis. In addition, whether the Warburg Micro syndrome is caused by deficiency of Rab18 mutants in responding to 2′3′-cGAMP regulation especially in driving neuronal migration critical in early development stages remains to be further determined.

We also find that lovastatin triggers Rab18 deprenylation that interrupts 2′3′-cGAMP binding and 2′3′-cGAMP–induced cell migration. Of note, there are multiple mechanisms underlying lovastatin treatment–induced cell migration changes other than Rab18 deprenylation. Different from 2′3′-cGAMP binding to the GTPase EF1A1 to suppress EF1A1 enzymatic activity by competing with GTP loading, 2′3′-cGAMP binding to the GTPase Rab18 coordinates with GTP loading to facilitate Rab18 activation. This study reveals an innate immunity-independent function of 2′3′-cGAMP and adds an additional consideration for disease treatments that include 2′3′-cGAMP. For example, Dox is a first-line therapy in treating triple-negative breast cancer (TNBC) but has a nonsatisfactory clinical outcome due to acquired resistance or lack of biomarkers. Our data suggest that TNBC treated with Dox may play a role in TNBC metastasis via activation of 2′3′-cGAMP/Rab18/FosB signaling. However, our data also suggest that this could be mitigated by lovastatin, a drug used to treat high cholesterol and triglyceride blood levels, and warrants further in-depth investigations.

Our studies rely on structure simulations to reveal possible binding features between Rab18 and 2′3′-cGAMP. Further crystallization of cryo–electron microscopy structures for the Rab18/2′3′-cGAMP or Rab18/2′3′-cGAMP/GTP complexes will be needed to provide the direct evidence for this interaction at atomic levels. We use *S. aureus* infection models to examine the contribution of increases of endogenous 2′3′-cGAMP in facilitating cell migration. To further strengthen this line of investigations, antibiotic-mediated depletion of tumor residing *S. aureus* or other bacterial species in a genetic of orthotopic breast cancer murine models would be necessary. Other limitations also exist. These include a lack of rigorous in vivo evidence of our identified 2′3′-cGAMP–induced cell migration control that could further provide tissue specificity and physiological significance for this signaling. This could be achieved by using a cre-loxp system to generate knockout strains for Rab18, cGAS, STING, or IRF3 with further crossing these animals with *Cre* mice specifically expressing Cre under a cell type–specific promoter. In addition, further efforts are warranted to complete the signaling cascade from 2′3′-cGAMP/Rab18 to FosB. Like other small GTPases as Ras, it is plausible that 2′3′-cGAMP–induced Rab18 activation triggers kinase activation to phosphorylate and stimulate transcription factors/coactivators to facilitate FosB transcription. Major FosB transcription target(s) responsible for 2′3′-cGAMP–governed cell migration control should be further determined in follow-up studies. Nonetheless, our study establishes a 2′3′-cGAMP/Rab18/FosB signaling in cell migration control and reveals pharmacological interventions by lovastatin to inhibit Rab18 prenylation alleviate 2′3′-cGAMP–induced cell migration, with both biological and pathological implications.

MATERIALS AND METHODS

Cell culture and transfection

Human breast cancer cell lines MDA-MB-231, MDA-MB-468, and T47D; human immortalized kidney cell line human embryonic kidney 293T, and MEFs were cultured in DMEM (Dulbecco's modified Eagle's medium) medium supplemented with 10% FBS, 100 U of penicillin, and streptomycin (100 mg/ml) unless otherwise stated. Human breast cancer cell lines HCC1937 and MDA-MB-436 and human leukemia monocytic cell line THP-1 were cultured in RPMI 1640 medium supplemented with 10% FBS, 100 U of penicillin, and streptomycin (100 mg/ml) unless otherwise stated.

Cell transfection was performed using polyethylenimine, as described previously (*48*, *49*). Packaging of lentiviral shRNA or cDNA expressing viruses, as well as subsequent infection of various cell lines, was performed according to the protocols described previously (*49*, *50*). Following viral infection, cells were maintained in the presence of blasticidin (5 μg/ml) or puromycin (1 μg/ml) or hygromycin (200 μg/ml) depending on the viral vector used to infect cells.

Bacteria strains

S. aureus HG003 MSSA strain and *GFP–S. aureus* BC47 LAC-GFP chromosome strain were gifts from B. Conlon (University of North Carolina at Chapel Hill). All strains were stored in 10% glycerol stock at −80°C. Cells were plated on tryptic soy broth agar plates (TSA) at 37°C overnight, and liquid suspensions of bacteria from the overnight culture were dilated to optical density at 600 nm = 0.6 and then used for further assays.

Plasmids

GST-Rab18-WT, S22N, Q67L, S17A, K98E, E68R, and R69AR71A were cloned into pGEX-6p-1 vector using Bam HI and Xho I enzyme sites. Hemagglutinin (HA)–Rab18–WT, HA-Rab18-S22N, HA-Rab18-Q67L, HA-Rab18-S17A, K98E, E68R, R69AR71A, and HA-Rab18-C203A were cloned into pLenti-GFP-blasticidin vector using Bam HI and Sal I enzyme sites. STING-WT-Flag and STING-R238A-Flag were cloned into pLenti-GFP-blasticidin vector using Bam HI and Sal I enzyme sites. S22N-Rab18, Q67L-Rab18, N122I-Rab18, S17A-Rab18, K98E-Rab18, E68R-Rab18, R69AR71A-Rab18, C203A-Rab18, and R238A-STING–related constructs were obtained using Site-Directed Mutagenesis Kits (Agilent, 200523).

Reagents

For transfection reagents and antibiotics, we purchased PEI from Polysciences Inc. (catalog no. 23866-1), blasticidin (Sigma-Aldrich, catalog no. 15205), puromycin (Fisher BioReagents, catalog no. 58-58-2), hygromycin (Sigma-Aldrich, catalog no. H3274), and gentamicin (Sigma-Aldrich, catalog no. G1264). As for nucleotide stimulants, we purchased ISD90 (5′-TACAGATCTACTAGTGATC-TATGACTGATCTGTACATGATCTACATACAGATCTACTAGT-GATCTATGACTGATCTGTACATGATCTACA-3′) from Eurofins Genomics. For other reagents used in this study, we purchased lovastatin from TCI America (catalog no. L0214), atorvastatin (TCI, catalog no. A2476), Dox (Fisher BioReagents, catalog no. BP2316-005), biotin-2′3′-cGAMP, (BioLOG, catalog no. c197-001), 3′2′-cGAMP (BioLOG, catalog no. c238-005), 3′3′-cGAMP (BioLOG, catalog no. c117-001), 2′3′-cGAMP (APExBio, catalog no. 88362), GTP solution (Thermo Fisher Scientific, catalog no. R0461), ActivX desthiobiotin-GTP probe (Thermo Fisher Scientific, catalog no. 88315), G140 (InvivoGen, catalog no. inh-g140), H-89 (AdipoGen, catalog no. 130964-39-5), compound C (Milipore, catalog no. 171260), neutravidin agarose beads (Thermo Fisher Scientific, catalog no. 29200), glutathione agarose beads (GE Healthcare, catalog no. 17-0756-05), anti-HA agarose beads (Sigma-Aldrich, catalog no. A-2095), and anti-Flag agarose beads (Sigma-Aldrich, catalog no. A2220), and cAMP was purchased from TCI (A2381), Alexa Fluor 594 phalloidin (Thermo Fisher Scientific, A12381), MRS-1706 (MCE, 264623-53-9), biotin-cAMP (AAT Bioquest, 17105), and 2′3′-cGAM(PS)$_2$ (Rp/Sp) (InvivoGen, catalog no. tlrl-nacga2srs-05). The Rneasy Mini Kit was purchased from QIAGEN (catalog no. 74106), iScript Reverse Transcription Supermix for qRT-PCR was from Bio-Rad (catalog no. 170-8891), Taq universal SYBR green supermix (Bio-Rad, catalog no. 172-5124), protease inhibitor cocktail (Bimake, catalog no. B14012), and phosphatase inhibitor cocktails A and B (Bimake, catalog no. B15001-A /B15001-B).

Antibodies

Antibodies used in this study were as follows: anti-HA-Tag antibody (Cell Signaling Technology, catalog no. 3724), anti-FosB antibody (Cell Signaling Technology, catalog no. 2251), anti-eEF1A1 antibody (Cell Signaling Technology, catalog no. 2551), anti–phospho-TBK1 (TANK binding kinase) (Ser^{172}) antibody (Cell Signaling Technology, catalog no. 5483), anti-TBK1 antibody (Cell Signaling Technology, catalog no. 51872), anti-STING antibody (Cell Signaling Technology, catalog no. 13647), anti–phospho-STING (Ser^{366}) antibody (Cell Signaling Technology, catalog no. 50907), anti-IRF3 antibody (Cell Signaling Technology, catalog no. 4302), anti–phospho-IRF3 (Ser^{386}) antibody (Cell Signaling Technology, catalog no. 37829), anti–phospho-IRF3 (Ser^{396}) antibody (Cell Signaling Technology, catalog no. 29047), anti-cGAS antibody (Cell Signaling Technology, catalog no. 83623), anti–phospho-histone H2A.X (Ser^{139}) (Cell Signaling Technology, catalog no. 9718), anti–GST-tag antibody (Santa Cruz Biotechnology, catalog no. sc-459), anti-Rab18 antibody (Santa Cruz Biotechnology, catalog no. sc-393169), anti–E-cadherin antibody (Santa Cruz Biotechnology, catalog no. sc-212791), anti-MMP9 (matrix metalloproteinase-9) antibody (Santa Cruz Biotechnology, catalog no. sc-21733), anti-Moesin antibody (Santa Cruz Biotechnology, catalog no. sc-13122), anti-SLUG antibody (Santa Cruz Biotechnology, catalog no. sc-166476), anti-MITF antibody (Santa Cruz Biotechnology, catalog no. sc-515925), anti-SNAI1 (snail family transcriptional repressor 1) antibody (Santa Cruz Biotechnology, catalog no. sc-271977), anti-SPARC antibody (Santa Cruz Biotechnology, catalog no. sc-398419), anti-TIMP1 (TIMP metallopeptidase inhibitor 1) antibody (Santa Cruz Biotechnology, catalog no. sc-365905), and anti–c-Jun antibody (Santa Cruz Biotechnology, catalog no. sc-1694); polyclonal anti-Flag antibody (Sigma-Aldrich, catalog no. F7425), monoclonal anti-Flag antibody (Sigma-Aldrich, catalog no. F-3165), monoclonal anti-tubulin antibody (Sigma-Aldrich, catalog no. T-5168), anti-vinculin antibody (Santa Cruz Biotechnology, catalog no. sc-25336), anti-GFP antibody (Abcam, ab13970), anti-LRRC8C antibody (Proteintech, 21601-1-AP), anti-SLC19A1 antibody (Proteintech, 25958-1-AP), anti-connexin43 (Proteintech, 26980-1-AP), anti-FAK (Proteintech, 12636-1-AP), anti-SLC46A2 (ABclonal, A15494), anti-RAB27A antibody (Proteintech, 17817-1-AP), anti-RAB3A antibody (Proteintech, 68052-2-Ig), anti-rabbit immunoglobulin G (IgG), horseradish peroxidase (HRP)–linked antibody (Cell Signaling Technology, catalog no. 7074), anti-mouse IgG, and HRP-linked antibody (Cell Signaling Technology, catalog no. 7076).

Primers

Primers used in generating plasmids used in this study are as follows: Rab18-HA-BamHI-F: GCAT GGATCC ATG TAC CCA TAC GAT GTT CCA GAT TAC GCT GACGAGGACGTGCTAACC; Rab18-BamHI-F: GCAT GGATCC GACGAGGACGTGCTAACC; Rab18-SalI-R: GCAT GTCGAC TTATAACACAGAGCAATA-ACCACCAC; Rab18-S22N-F: GAGAGTGGGGTGGGCAA-

GAACAGCCTGCTCTTGAGGTTC; Rab18-S22N-R: GAACCTCAAGAGCAGGCTGTTCTTGCCCACCCCACTCTC; Rab18-Q67L-F: CTTGCAATATGGGATACTGCTGGTCTAGAGAGGTTTAGAACATTAACTCC; Rab18-Q67L-R: GGAGTTAATGTTCTAAACCTCTCTAGACCAGCAGTATCCCATATTGCAAG; Rab18-N122I-F: CATAGTAAACATGCTAGTTGGAATCAAAATCGATAAGGAAAATCGTGAAG; Rab18-N122I-R: CTTCACGATTTTCCTTATCGATTTTGATTCCAACTAGCATGTTTACTATG; shRab18-79-resistant-F: GAAGGCCTGAAATTTGCTCGTAAACACTCGATGTTATTTATAGAGGCAAG; shRab18-79-resistant-R: CTTGCCTCTATAAATAACATCGAGTGTTTACGAGCAAATTTCAGGCCTTC; Rab18-S17A-F: CCTCATCATCGGCGAGGCTGGGGTGGGCAAGTCC; Rab18-S17A-R: GGACTTGCCCACCCCAGCCTCGCCGATGATGAGG; Rab18-E36A-F: CAGATGATACGTTTGATCCAGCACTTGCAGCAACAATAGGTGTTG; Rab18-E36A-R: CAACACCTATTGTTGCTGCAAGTGCTGGATCAAACGTATCATCTG; Rab18-R92E-F: GGTGTTATATTAGTTTATGATGTCACAGAAAGAGATACATTTGTTAAACTGGATAATTGG; Rab18-R92E-R: CCAATTATCCAGTTTAACAAATGTATCTCTTTCTGTGACATCATAAACTAATATAACACC; Rab18-K98E-F: CAAGAAGAGATACATTTGTTGAACTGGATAATTGGTTAAATGAATTGG; Rab18-K98E-R: CCAATTCATTTAACCAATTATCCAGTTCAACAAATGTATCTCTTCTTG; Rab18-E68K-F: GGATACTGCTGGTCAACGGAGGTTTAGAACATTAACTCCCAG; Rab18-E68K-R: CTGGGAGTTAATGTTCTAAACCTCCGTTGACCAGCAGTATCC; Rab18-R69AR71A-F: CTGCTGGTCAAGAGGCGTTTGCAACATTAACTCCCAGC; Rab18-R69AR71A-R: GCTGGGAGTTAATGTTGCAAACGCCTCTTGACCAGCAG; Rab18-C203A-R: GCATGTCGACTTATAACACAGAGGCATAACCACCAC; STING-R238A-F: GCTGGCATCAAGGATGCGGTTTACAGCAACAGCATCTATGAGC; STING-R238A-R: GCTCATAGATGCTGTTGCTGTAAACCGCATCCTTGATGCCAGC.

RT-PCR primers are as follows: NAB2-F: CCAGAGATGGTACGCATGGTG; NAB2-R: TTTAGCAGGGATGTGACCTCC; FosB-F: GCTGCAAGATCCCCTACGAAG; FosB-R: ACGAAGAAGTGTACGAAGGGTT; C3AR1-F: CCCTACGGCAGGTTCCTATG; C3AR1-R: GACAGCGATCCAGGCTAATGG; LIMA1-F: GACTCCCAGGTTAAGAGTGAGG; LIMA1-R: TTGCAGGTGCCTGAAACTTCT; U6-F: CTCGCTTCGGCAGCACA; U6-R: AACGCTTCACGAATTTGCGT; A2B-F: CAAGTGGGTGATGAATGTGG; A2B-R: TTTCCGGAATCAATTCAAGC; HK2-F: GAGTTTGACCTGGATGTGGTTGC; HK2-R: CCTCCATGTAGCAGGCATTGCT; c-FOS-F: GCCTCTCTTACTACCACTCACC; c-FOS-R: AGATGGCAGTGACCGTGGGAAT; CHGA-F: GGTTCTTGAGAACCAGAGCAGC; CHGA-R: GCTTCACCACTTTTCTCTGCCTC; FGF6-F: AGGCGTGGTGAGTCTCTTTGGA; FGF6-R: TTGTTGGGCAGGAGGGTTTCTC; AMD1-F: ACCACCCTCTTGCTGAAAGCAC; AMD1-R: CCCTTGGTGAGAAGGCTTCATG; SCG2-F: GAGAAGCCGAATGGATCAGTGG; SCG2-R: TCTGGATGGTCTAAGTCAGCCTC; JUND-F: ATCGACATGGACACGCAGGAGC; JUND-R: CTCCGTGTTCTGACTCTTGAGG; EGR2-F: CCTTTGACCAGATGAACGGAGTG; EGR2-R: GAAGGTCTGGTTTCTAGGTGCAG; PCNA-F: CAAGTAATGTCGATAAAGAGGAGG; PCNA-R: GTGTCACCGTTGAAGAGAGTGG; CALR-F: TCAAGGAGCAGTTTCTGGACGG; CALR-R: GCATCCTGGCTTGTCTGCAAAC; AREG-F: GCACCTGGAAGCAGTAACATGC; AREG-R: GGCAGCTATGGCTGCTAATGCA; KCNA5-F: GTTCCGCATCTTCAAGCTCTCC; KCNA5-R: CGAAGTAGACGGCACTGGAGAA.

shRNAs and sgRNAs

shRNA plasmids were constructed by inserting synthesized shRNAs into pLKO-puro or pLKO-blast vectors. Their target sequence is as follows: shSTING-28 (TRCN0000164628), shSTING-29 (TRCN0000163029), and shSTING-45 (TRCN0000161345); shRab10-M (TRCN0000382510), shRab10-N (TRCN0000379769), and shRab10-O (TRCN0000381036); shRab18-P (TRCN0000021979), shRab18-Q (TRCN0000021983), shRab18-R (TRCN0000021981), shRhoG-U (TRCN0000048018), shRhoG-S (TRCN0000048019), shRhoG-T (TRCN0000048021), shRRAGA-W (TRCN0000291754), shRRAGA-V (TRCN0000291692), shARHGEF1-A (TRCN0000033564), shARHGEF1-B (TRCN0000033567), shARHGEF1-C (TRCN0000033568), shRAP1GDS1-H (TRCN0000029789), shRAP1GDS1-G (TRCN0000029790), shRAP1GDS1-I (TRCN0000029792), shARHGEF2-D (TRCN0000003176), shARHGEF2-F (TRCN0000003173), shGAPVD1-J (TRCN0000010987), shGAPVD1-K (TRCN0000006005), shGAPVD1-L (TRCN0000006006), shmSTING-66 (TRCN0000346266), shmSTING-20 (TRCN0000346320), and shmSTING-64 (TRCN0000346264) constructs were purchased from Sigma-Aldrich. shRNA primers are listed as follows: shFosB-1: GCCGAGTCTCAATATCTGTCTC; shFosB-2: GCCAACCACAATTCAATGAAT; shA2B-F: CCGGGCTAATATGTATGTGTCAGTACTCGAGGCTAATATGTATGTGTCAGTATTTTTG; shA2B-R: AATTCAAAAAGCTAATATGTATGTGTCAGTACTCGAGGCTAATATGTATGTGTCAGTA.

sgRNA plasmids were constructed by inserting synthesized sgRNAs into lentiCRISPRv2-puro vector or lentiCRISPRv2-blast vector. Their target sequence is listed as follows: sgSTING-1: GCTGGGACTGCTGTTAAACG; sgSTING-2: GCGGGCCGACCGCATTTGGG; sgSTING-6: CATTACAACAACCTGCTACG; sgRab18-4: CCTCATCATCGGCGAGAGTG; sgEF1A1-1: GCTGTCCTGATTGTTGCTGC; sgEF1A1-2: AGGGCTCCTTCAAGTATGCC; sgEF1A1-3: GTTTCAGATGCCTTGGTTCA; sgFosB-1: CCGTAGGAGTGCGCCGGTCT; sgFosB-2: CGTCGACCCCTACGACATGC; sgIRF3-1: CGCTCACTGCCCAGTATGTG; sgIRF3-2: TTTAGCAGAGGACCGGAGCA; sgIRF3-4: GGCACCAACAGCCGCTTCAG.

sgRNA primers are listed as follows: sgLRRC8C-1-F: CACCGGACAAATGCCCATAATCGAC; sgLRRC8C-1-R: AAACGTCGATTATGGGCATTTGTCC; sgLRRC8C-2-F: CACCGCGTGCCTTTATACCTTATAC; sgLRRC8C-2-R: AAACGTATAAGGTATAAAGGCACGC; sgLRRC8C-3-F: CACCGATGCAACAAGATCCGATACT; sgLRRC8C-3-R: AAACAGTATCGGATCTTGTTGCATC; sgSLC46A2–1-F: CACCGCGTAGGACGCCTTCACCACG; sgSLC46A2–1-R: AAACCGTGGTGAAGGCGTCCTACGC; sgSLC46A2–2-F: CACCGAGCCCCGCATCGTAGAGGG; sgSLC46A2–2-R: AAACCCCTCTACGATGCGGGGCTC; sgSLC46A2–3-F: CACCGGGAGTAGCCCCGCATCGTAG; sgSLC46A2-3-R: AAACCTACGATGCGGGGCTACTCCC.

Immunoblot and immunoprecipitations analyses

Cells were lysed in EBC buffer [50 mM tris (pH 7.5), 120 mM NaCl, and 0.5% NP-40] supplemented with protease inhibitor cocktail and phosphatase inhibitor cocktail. The protein concentrations of whole cell lysates were measured by NanoDrop OneC using the Bio-Rad protein assay reagent as described previously (*48*, *49*). Equal amounts of whole cell lysates were loaded by SDS-PAGE and immunoblotted with indicated antibodies. For GST pull-down and immunoprecipitations analysis, 1 mg total lysates was incubated with the indicated beads for 3 to 4 hours at 4°C. The recovered immuno-complexes were

washed three times with NETN buffer [20 mM tris (pH 8.0), 100 mM NaCl, 1 mM EDTA, and 0.5% NP-40] before being resolved by SDS-PAGE and immunoblotted with indicated antibodies.

RNA extraction and qRT-PCR

RNA extraction was performed with an RNA miniprep super kit. The final elution step was done with 50 μl of ribonuclease-free water. The relative enrichment of mRNA was quantified with the NanoDrop OneC (Thermo Fisher Scientific). At least two biological replicates were performed for RNA extraction. Reverse transcription was performed with an iScript cDNA synthesis kit. Quantitative real-time PCR was performed with iTaq universal SYBR green supermix using a QuantStudio 6 Flex Real-Time PCR Systems (Thermo Fisher Scientific). Each mRNA level was normalized RNA18*S* to U6 small nuclear RNA. The comparative Ct method was used to calculate fold change in expression. Statistical significance was determined by one-way analysis of variance (ANOVA) tests.

RT^2 Profiler PCR assays

The RT^2 Profiler PCR array (330231 PAHS-066ZA) was purchased from QIAGEN. The assay was conducted following its instructions. Briefly, MDA-MB-231 cells were treated with vehicle/cGAMP for 2 hours followed by RNA extraction and cDNA synthesis, and then PCR component mix containing 2× SYBR Green mix and cDNA from each group was dispensed into PCR array followed by real-time PCR analysis as described previously.

Colony formation assays

Indicated cells were seeded into six-well plates (500 cells per well) and cultured in a 37°C incubator with 5% CO_2 for 10 to 15 days (as indicated in figure legends) until formation of visible colonies. Colonies were washed with 1× phosphate-buffered saline (PBS), fixed with 4% paraformaldehyde for 10 min, and stained with 0.5% crystal violet overnight. Colonies were then washed by distilled water and air-dried. Colony numbers were manually counted. Three independent experiments were performed to generate the error bars.

Transwell assays

A total of 3×10^4 or 3×10^5 cells were plated in an 8.0-mm, 24-well plate chamber insert (Corning Life Sciences, catalog no. 3422) with serum-free indicated medium at the top of the insert and the same medium containing 20% FBS or serum-free medium at the bottom of the insert unless otherwise stated. Cells were incubated for 24 hours and fixed with 4% paraformaldehyde for 10 min. After washing with PBS, cells at the top of the insert were scraped with a cotton swab. Cells adherent to the bottom were stained with 0.5% crystal violet blue for 60 min and then washed with double-distilled H_2O. The positively stained cells were examined under the microscope, and cell numbers were manually counted. Three independent experiments were performed to generate the error bars.

Biotin-2′3′-cGAMP pull-down assays

In vitro and in-cell pull-down assays were performed using biotin-2′3′-cGAMP (BioLOG) and NeutrAvidin agarose resin (Thermo Fisher Scientific). Cell lysates or recombinant GST-Rab18 proteins were incubated with 2 μg of biotin-2′3′-cGAMP and 10 liters of NeutrAvidin agarose beads in a total volume of 600 μl of EBC or NETN buffer for overnight at 4°C. The agarose beads were washed three times with NETN buffer. Then, bound proteins were eluted by boiling in SDS loading buffer and resolved by SDS-PAGE for subsequent staining by GelCode Blue (Thermo Fisher Scientific) or for Western blotting.

In vitro Desthiobiotin-GTP pull-down assays

In vitro pull-down assays were performed using Desthiobiotin-GTP probe (Thermo Fisher Scientific) and NeutrAvidin agarose resin (Thermo Fisher Scientific). Recombinant GST-Rab18 proteins were incubated with 20 μM Desthiobiotin-GTP and 10 liters of NeutrAvidin agarose beads in a total volume of 500 μl of binding buffer (50 mM tris-HCl, 250 mM NaCl, and 1% NP-40) for 4 to 6 hours at 4°C. The agarose beads were washed three times with binding buffer. Then, bound proteins were eluted by boiling in SDS loading buffer and resolved by SDS-PAGE for subsequent staining by GelCode Blue (Thermo Fisher Scientific) or for Western blotting.

In vitro biotin-cAMP pull-down assays

In vitro pull-down assays were performed using biotin-cAMP (AAT Bioquest) and NeutrAvidin agarose resin (Thermo Fisher Scientific). Recombinant GST-Rab18 proteins were incubated with 20 μM biotin-cAMP and 10 liters NeutrAvidin agarose beads in a total volume of 500 μl of binding buffer (50 mM tris-HCl, 250 mM NaCl, and 1% NP-40) for 4 to 6 hours at 4°C. The agarose beads were washed three times with binding buffer. Then, bound proteins were eluted by boiling in SDS loading buffer and resolved by SDS-PAGE for subsequent staining by GelCode Blue (Thermo Fisher Scientific) or for Western blotting.

Mass spectrometry

Sample preparation

cGAMP pull-down samples ($n = 2$; beads only control and biotin-2′3′-cGAMP pull-downs) were subjected to SDS-PAGE and stained with GelCode Blue Safe Protein Stain. Full lanes were analyzed (two gel slices per lane) and excised, and the proteins were reduced with 5 mM dithiothreitol (DTT), alkylated with 15 mM iodoacetamide, and in-gel digested with trypsin overnight at 37°C. Peptides were extracted, desalted with C18 ZipTip (Millipore), and dried via vacuum centrifugation. Peptide samples were stored at −80°C until further analysis.

LC-MS/MS analysis

The peptide samples ($n = 2$) were analyzed by liquid chromatography–tandem mass spectrometry (LC-MS/MS) using an Easy nLC 1200 coupled to a QExactive HF mass spectrometer (Thermo Fisher Scientific). Samples were injected onto an Easy Spray PepMap C18 column (75 μm id by 25 cm, 2-μm particle size) (Thermo Fisher Scientific) and separated over a 65-min method. The gradient for separation consisted of 5 to 40% mobile phase B at a 250 nl/min flow rate, where mobile phase A was 0.1% formic acid in water and mobile phase B consisted of 0.1% formic acid in 80% acetonitrile (ACN). The QExactive HF was operated in data-dependent mode where the 15 most intense precursors were selected for subsequent fragmentation. Resolution for the precursor scan (mass/charge ratio 400 to 1600) was set to 120,000 with a target value of 3×10^6 ions. MS/MS scan resolution was set to 15,000 with a target value of 5×10^4 ions. The normalized collision energy was set to 27% for higher collisional dissociation (HCD). Dynamic exclusion was set to 30 s, peptide match was set to preferred, and

precursors with unknown charge or a charge state of 1 and ≥8 were excluded.

Data analysis

Raw data files were processed using Proteome Discoverer version 2.1 (Thermo Fisher Scientific). Peak lists were searched against a reviewed UniProt human database (downloaded April 2017, containing 20,378 entries) appended with a common contaminant database. The following parameters were used to identify tryptic peptides for protein identification: 10–parts per million precursor ion mass tolerance; 0.02-Da product ion mass tolerance; up to two missed trypsin cleavage sites; carbamidomethylation of Cys was set as a fixed modification; oxidation of Met and protein N-terminal acetyl were set as a variable modification.

Scaffold (version 4.7.3, Proteome Software) was used to validate MS/MS-based peptide and protein identifications and to provide relative quantitation. Peptide identifications were accepted if they could be established at greater than 95% probability to achieve a false discovery rate of less than 0.1% by the Scaffold Local FDR algorithm. Protein identifications were accepted if they could be established at greater than 95.0% probability and contained at least two identified peptides. Relative quantitation was performed using the calculated quantitative values (spectral counts) within Scaffold.

CB-Dock modeling of 2′3′-cGAMP binding to Rab18

CB-Dock (http://clab.labshare.cn/cb-dock/php/index.php) is a protein-ligand docking method which explores the protein surface for binding sites, automatically identifies and characterizes potential binding sites, and then uses AutoDock Vina (http://vina.scripps.edu) to dock the ligand into the identified binding sites. The ligand used was cGAMP from the 3.0-Å crystal structure of a mutant hSTING in complex with 2′,3′-cGAMP (PDB: 6y99). The protein used was a monomer of apo-hRab18 from a 1.32-Å crystal structure of hRab18 in complex with Gppnhp (PDB: 1x3s). The top docking pose from CB-Dock is rendered in Fig. 3. Rab18 is rendered in slate as a cartoon with three residues predicted to make contact to cGAMP (S17, E36, and R92) rendered as sticks and colored by atom-type. cGAMP is rendered as sticks, colored by atom type with carbons colored white. The solved crystal structure of Rab18 binding to Gppnhp (nondegradable GTP) (PDB: 1x3s) was used as the input in the PrankWeb server. Two binding pockets were identified by PrankWeb as shown in fig. S6. A third pocket was selected as a negative control by choosing a cave-like area on the surface of Rab18. 2′3′-cGAMP, 3′2′-cGAMP, or 3′3′-cGAMP was then docked to these binding pockets by using MedusaDock. One thousand docking attempts were performed at each pocket. Last, the 1000 generated ligand poses were clustered by MedusaDock, and the centroid of the largest cluster was selected as the final stable pose at each pocket.

Rab18 GTPase activity assays

The in vitro GTPase activity assays using GST-Rab18 proteins were performed using the ATPase/GTPase Activity Assay kit (MAK113, Sigma-Aldrich) following manufacturer's instructions. Briefly, bacterially purified GST-Rab18 proteins was incubated GTP (1 mM) using a 96-well plate for 30 min or indicated time at room temperature or 37°C and then incubated with the reagent for an additional 30 min at room temperature to stop the enzyme reaction and generate the colorimetric product, and then samples were read at A_{620}.

Immunofluorescence

Cells plated onto glass coverslips were fixed with 4% paraformaldehyde in PBS for 20 min at room temperature and permeabilized with 0.2% Triton X-100 for 20 min at room temperature. Cells were incubated with blocking buffer (5% bovine serum albumin and 0.1% Triton X-100 in PBS) for 1 hour, incubated with primary antibodies at 4°C overnight, incubated with secondary antibodies at room temperature for 1 hour, and mounted with ProLong Gold antifade reagent. Fluorescent signals were observed with a Keyence BZ-X700 microscope.

Oil Red O staining

Cells plated in a 24-well plate were washed two times with PBS and fixed with 10% formalin for 30 min at room temperature. After removing formalin and washing two times with distilled H_2O (dH_2O), cells were incubated with 60% isopropanol for 5 min, Oil Red O solution for 30 min, and hematoxylin for 1 min. Cells were kept with dH_2O at all times including while viewed under the microscope.

Protein purification

The recombinant GST-Rab18 was expressed in *Escherichia coli* BL21 strain with isopropyl β-D-1-thiogalactopyranoside induction 16 hours at 16°C. The bacteria pellets were resuspended in lysis buffer (with protease inhibitor in PBS) and cracked by sonication. Following centrifugation for 30 min at 16,000*g* to get rid of the bacteria debris, prewashed GST-sepharose beads slurry (GE Healthcare) were added to the supernatant and then incubated for 4 hours at 4°C. Proteins were eluted by elution buffer [20 mM reduced glutathione in 50 mM tris-HCl (pH 8.0)]. Where indicated, GST tag was removed by protease cleavage, and the final products were purified and validated by fast protein liquid chromatography size exclusion chromatography and gel analyses.

GST-Rab18 tag cleavage

After elution from the GST column, GST-Rab18 was exchanged into PBS buffer with 5 mM BME and concentrated to 1.8 ml. The protein was digested with 50 U of ApexBio Precision protease in provided cleavage buffer for 48 hours at 4°C. Following cleavage, the protein was reloaded onto the GST column. Rab18 proteins were collected in the flow-through and one column volume PBS wash. The protein was concentrated to 0.5 ml, quantified, and exchanged into 32 mM tris (pH 8.0), 200 mM ammonium sulfate, 10 mM DTT, and 0.15% *N*-octylglucopyranoside using a preequilibrated PD10 column (Cytiva) by gravity flow. Fractions containing Rab18 were identified via a quick nonquantitative Bradford assay and pooled to approximately 2 ml. Passenger nucleotides were exchanged out in the presence of 10 mg of GppNHp and 25 U of alkaline phosphatase (AP) beads (Sigma-Aldrich) per milligram Rab18 at 37°C for 60 min with gentle mixing. $MgCl_2$ (20 mM; final concentration) was added to the protein slurry and incubated for 5 min. The AP beads were removed via centrifugation. Last, the protein was exchanged into 20 mM Hepes, 50 mM NaCl, 20 mM $MgCl_2$, and 1 mM TCEP using a preequilibrated PD10 column as above.

Enzyme-linked immunosorbent assay

Enzyme-linked immunosorbent assays (ELISAs) for human 2′3′-cGAMP and 3′3′-cGAMP were performed using cell lysates in which values are expressed as picograms per milliliter or nanograms per milliliter ± SD as calculated from a standard curve derived from

2′3′-cGAMP or 3′3′-cGAMP provided in the ELISA kit (2′3′-cGAMP ELISA, 501700, Cayman Chemical; 3′3′-cGAMP ELISA, 502130, Cayman Chemical).

RNA-seq analyses of 2′3′-cGAMP–governed transcriptome

Total RNA from triplicated samples of THP1-*STING*$^{-/-}$ cells treated with or without 2′3′-cGAMP (5 μg/ml) was extracted with the QIAGEN RNeasy mini kit. Library preparation and sequencing were performed by NOVOgene as paired-end 150-bp reads. Reads were then filtered for adaptor contamination using cutadapt and filtered such that at least 90% of bases of each read had a quality score > 30. Reads were aligned to the reference genome (hg19) using STAR version 2.5.2b retaining only primary alignments (*51*). Reads overlapping blacklisted regions of the genome were then removed. Transcript abundance was then estimated using Salmon (*52*), and differentially expressed genes were detected using DESeq2 with the criteria of adjusted *P* values (adj*P*) < 0.05 (*53*). The ClusterProfiler R package (v3.14.3) was used to analyze the Gene Ontology (GO) and Kyoto Encyclopedia of Genes and Genomes (KEGG) for functional pathway annotation. Enrichment analysis for GO terms and KEGG pathways uses enrichGO and enrichKEGG functions and visualizes the result with bubble plots. RNA-seq data are deposited to GEO under accession number GSE210490.

MTT cell viability assay

Two thousand indicated cells were seeded in each well of 96-well plates for MTT assays to monitor cell viability at indicated time periods. Briefly, at indicated time points postcell seeding, 10 ml of MTT solution was added into each well and incubated in the culture incubator (37°C with 5% CO_2) for 4 hours. Then, medium was removed, and 100 ml of dimethyl sulfoxide was added into each well to dissolve the formazan crystal and incubated for 10 min at 37°C. After thorough mixing, absorbance at 540 nm was measured using the BioTek Cytation 5 Cell Imaging reader.

Time-lapse imaging

Indicated cells were seeded in a six-well plate for time-lapse cell movement assay. After cells were attached, 2′3′-cGAMP (2.5 μg/ml) was added to indicated wells and recorded for 16 to 24 hours with 30- or 60-min intervals. Time-lapse movies were recorded by the EVOS M7000 microscope Imaging system or the Incucyte Live-Cell Analysis System and generated by Fiji. Briefly, *x* and *y* coordinates of each cell were measured by every time point, and the total cell movement distances were calculated by the measurements. Statistical significance was determined by one-way ANOVA tests.

Mouse tail vein injection assays

All mouse work has been reviewed and approved by UNC Institutional Animal Care and Use Committee under IACUC#22-056. Briefly, MDA-MB-231-luc cells were treated with vehicle, G140 (10 μM), or Dox (0.05 μM) + lovastatin (5 μM) for 24 hours, and then 5×10^5 cells from each group were collected and resuspended in 100 μl of PBS and injected into tail veins of 6-week-old NSG mice purchased through the UNC Lineberger Comprehensive Cancer Center (LCCC) Animal Studies Core. The core facility was blinded for this measurement. MDA-MB-231-luc-shscramble/shRab18 cells were treated with vehicle, *S. aureus* for 6 hours followed by treatment with gentamicin for 1 hours, and then 3×10^5 cells from each group were collected and resuspended in 100 μl of PBS and injected into tail veins of 9-week-old NSG mice purchased through the UNC LCCC Animal Studies Core. MDA-MB-231-luc cells were treated with vehicle or lovastatin (5 μM) for 24 hours postinjection, and 3×10^5 cells from each group were collected and resuspended in 100 μl of PBS and injected into tail veins of 7-week-old NSG mice purchased through the UNC LCCC Animal Studies Core. Cell metastasis to lung was monitored two to three times a week by noninvasive imaging. Animals were euthanized if more than 20% weight loss was observed and excluded from the experiments.

In vitro binding assay

In vitro binding assay was performed using biotin-2′3′-cGAMP (BioLOG-C197) and NeutrAvidin agarose resin (Thermo Fisher Scientific). Recombinant GST-Rab18 (50 mM) proteins were incubated with different doses (0 to 100 μM) of biotin-2′3′-cGAMP and 5 μl of NeutrAvidin agarose beads in a total volume of 20 μl of EBC buffer for 1 hour at 4°C. The agarose beads were washed three times with EBC buffer. Then, bound proteins were eluted by boiling in SDS loading buffer and resolved by SDS-PAGE for subsequent Western blotting. The density of resulting bands was quantified using imageJ, and dissociation constants (K_d value) and R^2 values were calculated using GraphPad Prism (one-side--pecific binding).

In vitro HSV-1 transwell assays

A total of 3×10^5 or 4×10^5 per well MDA-MB-231 cells were plated in 24-well plates and infected by purified HSV-1 at a multiplicity of infection (MOI) of 0 or 0.5 for 1 hour followed by refreshing media for another 48-hour incubation. Then, the supernatants from indicated conditions were collected for transwell assays. For G140 inhibition assay, 4×10^5 per well MDA-MB-231 cells were plated in a 24-well plate. Before infected by HSV-1 (MOI = 0.5), cells were pretreated with G140 (10 μM) for 1 hour. After 1 hour of HSV-1 infection, medium was refreshed that contains G140 (10 μM) for another 48-hour incubation. Then, the supernatants from different conditions were collected for transwell assays.

Statistical analyses

Statistical analyses were performed using the SPSS 11.5 Statistical Software. $P \leq 0.05$ was considered statistically significant. The results are shown as means ± SD from at least two or three independent experiments as indicated in figure legends. Differences between control and experimental conditions were evaluated by one-way ANOVA.

Supplementary Materials

The PDF file includes:

Figs. S1 to S10
Table S1
Legends for movies S1 and S2

Other Supplementary Material for this manuscript includes the following:

Movies S1 and S2

REFERENCES AND NOTES

1. M. Gomelsky, cAMP, c-di-GMP, c-di-AMP and now cGMP: Bacteria use them all! *Mol. Microbiol.* **79**, 562–565 (2011).
2. U. Romling, M. Y. Galperin, M. Gomelsky, Cyclic di-GMP: The first 25 years of a universal bacterial second messenger. *Microbiol. Mol. Biol. Rev.* **77**, 1–52 (2013).
3. D. Cohen, S. Melamed, A. Millman, G. Shulman, Y. Oppenheimer-Shaanan, A. Kacen, S. Doron, G. Amitai, R. Sorek, Cyclic GMP-AMP signalling protects bacteria against viral infection. *Nature* **574**, 691–695 (2019).

4. A. Ren, X. C. Wang, C. A. Kellenberger, K. R. Rajashankar, R. A. Jones, M. C. Hammond, D. J. Patel, Structural basis for molecular discrimination by a 3′,3'-cGAMP sensing riboswitch. *Cell Rep.* **11**, 1–12 (2015).
5. X. Zhang, H. Shi, J. Wu, X. Zhang, L. Sun, C. Chen, Z. J. Chen, Cyclic GMP-AMP containing mixed phosphodiester linkages is an endogenous high-affinity ligand for STING. *Mol. Cell* **51**, 226–235 (2013).
6. L. Sun, J. Wu, F. Du, X. Chen, Z. J. Chen, Cyclic GMP-AMP synthase is a cytosolic DNA sensor that activates the type I interferon pathway. *Science* **339**, 786–791 (2013).
7. L. Corrales, S. M. McWhirter, T. W. Dubensky Jr., T. F. Gajewski, The host STING pathway at the interface of cancer and immunity. *J. Clin. Invest.* **126**, 2404–2411 (2016).
8. G. N. Barber, STING: Infection, inflammation and cancer. *Nat. Rev. Immunol.* **15**, 760–770 (2015).
9. J. Vincent, C. Adura, P. Gao, A. Luz, L. Lama, Y. Asano, R. Okamoto, T. Imaeda, J. Aida, K. Rothamel, T. Gogakos, J. Steinberg, S. Reasoner, K. Aso, T. Tuschl, D. J. Patel, J. F. Glickman, M. Ascano, Small molecule inhibition of cGAS reduces interferon expression in primary macrophages from autoimmune mice. *Nat. Commun.* **8**, 750 (2017).
10. H. Wang, S. Hu, X. Chen, H. Shi, C. Chen, L. Sun, Z. J. Chen, cGAS is essential for the antitumor effect of immune checkpoint blockade. *Proc. Natl. Acad. Sci. U.S.A.* **114**, 1637–1642 (2017).
11. Y. Hou, H. Lu, J. Li, Z. Guan, J. Zhang, W. Zhang, C. Yin, L. Sun, Y. Zhang, H. Jiang, A photoaffinity labeling strategy identified EF1A1 as a binding protein of cyclic dinucleotide 2′3′-cGAMP. *Cell Chem. Biol.* **29**, 133–144.e20 (2021).
12. K. Sureka, P. H. Choi, M. Precit, M. Delince, D. A. Pensinger, T. N. Huynh, A. R. Jurado, Y. A. Goo, M. Sadilek, A. T. Iavarone, J. D. Sauer, L. Tong, J. J. Woodward, The cyclic dinucleotide c-di-AMP is an allosteric regulator of metabolic enzyme function. *Cell* **158**, 1389–1401 (2014).
13. T. B. Cereija, J. P. L. Guerra, J. M. P. Jorge, J. H. Morais-Cabral, c-di-AMP, a likely master regulator of bacterial K^+ homeostasis machinery, activates a K^+ exporter. *Proc. Natl. Acad. Sci. U. S. A.* **118**, e2020653118 (2021).
14. J. Stulke, L. Kruger, Cyclic di-AMP Signaling in Bacteria. *Annu. Rev. Microbiol.* **74**, 159–179 (2020).
15. C. R. Justus, N. Leffler, M. Ruiz-Echevarria, L. V. Yang, In vitro cell migration and invasion assays. *J. Vis. Exp.* **88**, 51046 (2014).
16. J. Pijuan, C. Barcelo, D. F. Moreno, O. Maiques, P. Siso, R. M. Marti, A. Macia, A. Panosa, In vitro cell migration, invasion, and adhesion assays: From cell imaging to data analysis. *Front. Cell Dev. Biol.* **7**, 107 (2019).
17. C. Zhou, X. Chen, R. Planells-Cases, J. Chu, L. Wang, L. Cao, Z. Li, K. I. Lopez-Cayuqueo, Y. Xie, S. Ye, X. Wang, F. Ullrich, S. Ma, Y. Fang, X. Zhang, Z. Qian, X. Liang, S. Q. Cai, Z. Jiang, D. Zhou, Q. Leng, T. S. Xiao, K. Lan, J. Yang, H. Li, C. Peng, Z. Qiu, T. J. Jentsch, H. Xiao, Transfer of cGAMP into bystander cells via LRRC8 volume-regulated anion channels augments STING-mediated interferon responses and anti-viral immunity. *Immunity* **52**, 767–781.e766 (2020).
18. L. J. Lahey, R. E. Mardjuki, X. Wen, G. T. Hess, C. Ritchie, J. A. Carozza, V. Bohnert, M. Maduke, M. C. Bassik, L. Li, LRRC8A:C/E heteromeric channels are ubiquitous transporters of cGAMP. *Mol. Cell* **80**, 578–591.e575 (2020).
19. A. F. Cordova, C. Ritchie, V. Bohnert, L. Li, Human SLC46A2 is the dominant cGAMP importer in extracellular cGAMP-sensing macrophages and monocytes. *ACS Cent. Sci.* **7**, 1073–1088 (2021).
20. C. Ritchie, A. F. Cordova, G. T. Hess, M. C. Bassik, L. Li, SLC19A1 is an importer of the immunotransmitter cGAMP. *Mol. Cell* **75**, 372–381.e375 (2019).
21. R. D. Luteijn, S. A. Zaver, B. G. Gowen, S. K. Wyman, N. E. Garelis, L. Onia, S. M. McWhirter, G. E. Katibah, J. E. Corn, J. J. Woodward, D. H. Raulet, SLC19A1 transports immunoreactive cyclic dinucleotides. *Nature* **573**, 434–438 (2019).
22. G. Pepin, D. De Nardo, C. L. Rootes, T. R. Ullah, S. S. Al-Asmari, K. R. Balka, H. M. Li, K. M. Quinn, F. Moghaddas, S. Chappaz, B. T. Kile, E. F. Morand, S. L. Masters, C. R. Stewart, B. R. G. Williams, M. P. Gantier, Connexin-dependent transfer of cGAMP to phagocytes modulates antiviral responses. *mBio* **11**, e03187-19 (2020).
23. L. Li, Q. Yin, P. Kuss, Z. Maliga, J. L. Millan, H. Wu, T. J. Mitchison, Hydrolysis of 2′3′-cGAMP by ENPP1 and design of nonhydrolyzable analogs. *Nat. Chem. Biol.* **10**, 1043–1048 (2014).
24. J. Li, M. A. Duran, N. Dhanota, W. K. Chatila, S. E. Bettigole, J. Kwon, R. K. Sriram, M. P. Humphries, M. Salto-Tellez, J. A. James, M. G. Hanna, J. C. Melms, S. Vallabhaneni, K. Litchfield, I. Usaite, D. Biswas, R. Bareja, H. W. Li, M. L. Martin, P. Dorsaint, J. A. Cavallo, P. Li, C. Pauli, L. Gottesdiener, B. J. DiPardo, T. J. Hollmann, T. Merghoub, H. Y. Wen, J. S. Reis-Filho, N. Riaz, S. M. Su, A. Kalbasi, N. Vasan, S. N. Powell, J. D. Wolchok, O. Elemento, C. Swanton, A. N. Shoushtari, E. E. Parkes, B. Izar, S. F. Bakhoum, Metastasis and immune evasion from extracellular cGAMP hydrolysis. *Cancer Discov.* **11**, 1212–1227 (2021).
25. M. Fernandez-Gallardo, R. Gonzalez-Ramirez, A. Sandoval, R. Felix, E. Monjaraz, Adenosine stimulate proliferation and migration in triple negative breast cancer cells. *PLOS One* **11**, e0167445 (2016).
26. Y. Sun, P. Huang, Adenosine A2B Receptor: From cell biology to human diseases. *Front. Chem.* **4**, 37 (2016).
27. P. Gao, M. Ascano, T. Zillinger, W. Wang, P. Dai, A. A. Serganov, B. L. Gaffney, S. Shuman, R. A. Jones, L. Deng, G. Hartmann, W. Barchet, T. Tuschl, D. J. Patel, Structure-function analysis of STING activation by c[G(2′,5′)pA(3′,5′)p] and targeting by antiviral DMXAA. *Cell* **154**, 748–762 (2013).
28. L. Lama, C. Adura, W. Xie, D. Tomita, T. Kamei, V. Kuryavyi, T. Gogakos, J. I. Steinberg, M. Miller, L. Ramos-Espiritu, Y. Asano, S. Hashizume, J. Aida, T. Imaeda, R. Okamoto, A. J. Jennings, M. Michino, T. Kuroita, A. Stamford, P. Gao, P. Meinke, J. F. Glickman, D. J. Patel, T. Tuschl, Development of human cGAS-specific small-molecule inhibitors for repression of dsDNA-triggered interferon expression. *Nat. Commun.* **10**, 2261 (2019).
29. Y. Hou, H. Lu, J. Li, Z. Guan, J. Zhang, W. Zhang, C. Yin, L. Sun, Y. Zhang, H. Jiang, A photoaffinity labeling strategy identified EF1A1 as a binding protein of cyclic dinucleotide 2′3′-cGAMP. *Cell Chem. Biol.* **29**, 133–144.e120 (2022).
30. M. Parri, P. Chiarugi, Rac and Rho GTPases in cancer cell motility control. *Cell Commun. Signal* **8**, 23 (2010).
31. J. Wang, A. Jain, L. R. McDonald, C. Gambogi, A. L. Lee, N. V. Dokholyan, Mapping allosteric communications within individual proteins. *Nat. Commun.* **11**, 3862 (2020).
32. N. A. Guadagno, A. Margiotta, S. A. Bjornestad, L. H. Haugen, I. Kjos, X. Xu, X. Hu, O. Bakke, F. Margadant, C. Progida, Rab18 regulates focal adhesion dynamics by interacting with kinectin-1 at the endoplasmic reticulum. *J. Cell Biol.* **219**, e201809020 (2020).
33. J. Kim, S. M. Kang, S. Y. Oh, H. J. Lee, I. Lee, J. C. Hwang, S. H. Hong, NGFI-A binding protein 2 promotes EGF-dependent HNSCC cell invasion. *Cancers* **11**, 315 (2019).
34. C. S. Barrett, A. C. Millena, S. A. Khan, TGF-beta effects on prostate cancer cell migration and invasion require FosB. *Prostate* **77**, 72–81 (2017).
35. S. Hannedouche, V. Beck, J. Leighton-Davies, M. Beibel, G. Roma, E. J. Oakeley, V. Lannoy, J. Bernard, J. Hamon, S. Barbieri, I. Preuss, M. C. Lasbennes, A. W. Sailer, T. Suply, K. Seuwen, C. N. Parker, F. Bassilana, Identification of the C3a receptor (C3AR1) as the target of the VGF-derived peptide TLQP-21 in rodent cells. *J. Biol. Chem.* **288**, 27434–27443 (2013).
36. S. Zhang, X. Wang, A. O. Osunkoya, S. Iqbal, Y. Wang, Z. Chen, S. Muller, Z. Chen, S. Josson, I. M. Coleman, P. S. Nelson, Y. A. Wang, R. Wang, D. M. Shin, F. F. Marshall, O. Kucuk, L. W. Chung, H. E. Zhau, D. Wu, EPLIN downregulation promotes epithelial-mesenchymal transition in prostate cancer cells and correlates with clinical lymph node metastasis. *Oncogene* **30**, 4941–4952 (2011).
37. D. Nejman, I. Livyatan, G. Fuks, N. Gavert, Y. Zwang, L. T. Geller, A. Rotter-Maskowitz, R. Weiser, G. Mallel, E. Gigi, A. Meltser, G. M. Douglas, I. Kamer, V. Gopalakrishnan, T. Dadosh, S. Levin-Zaidman, S. Avnet, T. Atlan, Z. A. Cooper, R. Arora, A. P. Cogdill, M. A. W. Khan, G. Ologun, Y. Bussi, A. Weinberger, M. Lotan-Pompan, O. Golani, G. Perry, M. Rokah, K. Bahar-Shany, E. A. Rozeman, C. U. Blank, A. Ronai, R. Shaoul, A. Amit, T. Dorfman, R. Kremer, Z. R. Cohen, S. Harnof, T. Siegal, E. Yehuda-Shnaidman, E. N. Gal-Yam, H. Shapira, N. Baldini, M. G. I. Langille, A. Ben-Nun, B. Kaufman, A. Nissan, T. Golan, M. Dadiani, K. Levanon, J. Bar, S. Yust-Katz, I. Barshack, D. S. Peeper, D. J. Raz, E. Segal, J. A. Wargo, J. Sandbank, N. Shental, R. Straussman, The human tumor microbiome is composed of tumor type-specific intracellular bacteria. *Science* **368**, 973–980 (2020).
38. A. Fu, B. Yao, T. Dong, Y. Chen, J. Yao, Y. Liu, H. Li, H. Bai, X. Liu, Y. Zhang, C. Wang, Y. Guo, N. Li, S. Cai, Tumor-resident intracellular microbiota promotes metastatic colonization in breast cancer. *Cell* **185**, 1356–1372.e1326 (2022).
39. S. Skopelja-Gardner, J. An, K. B. Elkon, Role of the cGAS-STING pathway in systemic and organ-specific diseases. *Nat. Rev. Nephrol.* **18**, 558–572 (2022).
40. B. Wei, L. Xu, W. Guo, Y. Wang, J. Wu, X. Li, X. Cai, J. Hu, M. Wang, Q. Xu, W. Liu, Y. Gu, SHP2-mediated inhibition of DNA repair contributes to cGAS-STING activation and chemotherapeutic sensitivity in colon cancer. *Cancer Res.* **81**, 3215–3228 (2021).
41. R. A. Alcock, S. Dey, D. Chendil, M. S. Inayat, M. Mohiuddin, G. Hartman, L. K. Chatfield, V. S. Gallicchio, M. M. Ahmed, Farnesyltransferase inhibitor (L-744,832) restores TGF-beta type II receptor expression and enhances radiation sensitivity in K-ras mutant pancreatic cancer cell line MIA PaCa-2. *Oncogene* **21**, 7883–7890 (2002).
42. J. Gao, J. Liao, G. Y. Yang, CAAX-box protein, prenylation process and carcinogenesis. *Am. J. Transl. Res.* **1**, 312–325 (2009).
43. B. Wu, R. Qi, X. Liu, L. Qian, Z. Wu, Rab18 overexpression promotes proliferation and chemoresistance through regulation of mitochondrial function in human gastric cancer. *Onco. Targets. Ther.* **11**, 7805–7820 (2018).
44. T. Gong, B. Zhou, M. Liu, X. Chen, S. Huang, Y. Xu, R. Luo, Z. Chen, RAB18 promotes proliferation and metastasis in hepatocellular carcinoma. *Am. J. Transl. Res.* **11**, 1009–1019 (2019).
45. K. Zhong, K. Chen, L. Han, B. Li, MicroRNA-30b/c inhibits non-small cell lung cancer cell proliferation by targeting Rab18. *BMC Cancer* **14**, 703 (2014).
46. D. Bem, S. Yoshimura, R. Nunes-Bastos, F. C. Bond, M. A. Kurian, F. Rahman, M. T. Handley, Y. Hadzhiev, I. Masood, A. A. Straatman-Iwanowska, A. R. Cullinane, A. McNeill, S. S. Pasha, G. A. Kirby, K. Foster, Z. Ahmed, J. E. Morton, D. Williams, J. M. Graham, W. B. Dobyns, L. Burglen, J. R. Ainsworth, P. Gissen, F. Muller, E. R. Maher, F. A. Barr, I. A. Aligianis,

Loss-of-function mutations in RAB18 cause Warburg micro syndrome. *Am. J. Hum. Genet.* **88**, 499–507 (2011).
47. M. Qi, L. A. Sun, L. R. Zheng, J. Zhang, Y. L. Han, F. Wu, J. Zhao, W. H. Niu, M. X. Fei, X. C. Jiang, M. L. Zhou, Expression and potential role of FOSB in glioma. *Front. Mol. Neurosci.* **15**, 972615 (2022).
48. S. Su, J. Chen, Y. Jiang, Y. Wang, T. Vital, J. Zhang, C. Laggner, K. T. Nguyen, Z. Zhu, A. W. Prevatte, N. K. Barker, L. E. Herring, I. J. Davis, P. Liu, SPOP and OTUD7A control EWS-FLI1 protein stability to govern Ewing sarcoma growth. *Adv. Sci.* **8**, e2004846 (2021).
49. Y. Jiang, Y. Zhang, J. Y. Leung, C. Fan, K. I. Popov, S. Su, J. Qian, X. Wang, A. Holtzhausen, E. Ubil, Y. Xiang, I. Davis, N. V. Dokholyan, G. Wu, C. M. Perou, W. Y. Kim, H. S. Earp, P. Liu, MERTK mediated novel site Akt phosphorylation alleviates SAV1 suppression. *Nat. Commun.* **10**, 1515 (2019).
50. P. Liu, M. Begley, W. Michowski, H. Inuzuka, M. Ginzberg, D. Gao, P. Tsou, W. Gan, A. Papa, B. M. Kim, L. Wan, A. Singh, B. Zhai, M. Yuan, Z. Wang, S. P. Gygi, T. H. Lee, K. P. Lu, A. Toker, P. P. Pandolfi, J. M. Asara, M. W. Kirschner, P. Sicinski, L. Cantley, W. Wei, Cell-cycle-regulated activation of Akt kinase by phosphorylation at its carboxyl terminus. *Nature* **508**, 541–545 (2014).
51. A. Dobin, C. A. Davis, F. Schlesinger, J. Drenkow, C. Zaleski, S. Jha, P. Batut, M. Chaisson, T. R. Gingeras, STAR: Ultrafast universal RNA-seq aligner. *Bioinformatics* **29**, 15–21 (2013).
52. R. Patro, G. Duggal, M. I. Love, R. A. Irizarry, C. Kingsford, Salmon provides fast and bias-aware quantification of transcript expression. *Nat. Methods* **14**, 417–419 (2017).
53. M. I. Love, W. Huber, S. Anders, Moderated estimation of fold change and dispersion for RNA-seq data with DESeq2. *Genome Biol.* **15**, 550 (2014).

Acknowledgments: We thank P.L. lab members for critical reading of the manuscript and helpful discussions. We sincerely thank J. Ting and Z. James Chen for helpful suggestions. We also thank X. Zhou and G. Dotti from University of North Carolina at Chapel Hill with tail vein injections. Animal studies were performed within the UNC Lineberger Animal Study Core at the University of North Carolina at Chapel Hill which is supported in part by an NCI Center Core Support Grant (CA16086) to the UNC Lineberger Comprehensive Cancer Center. We thank the Small Animal Imaging Core Facility at the UNC Biomedical Imaging Research Center for providing optical imaging service. The imaging core is supported in part by NIH grant P30CA016086, and the IVIS imaging system was funded by an NIH grant, S10OD026951. **Funding:** This work was supported by a National Institutes of Health R01 CA244825 (P.L.), the Mary Kay Ash Foundation (P.L.), the Gabrielle's Angel Foundation Medical Research Award (P.L.), the University of North Carolina at Chapel Hill University Cancer Research Fund (P.L.), National Institutes of Health grants CA019014 and CA163217 (B.D.), a National Institutes of Health no. 1R35 GM134864, 1RF1 AG071675) (N.V.D.), and the Passan Foundation at Penn State College of Medicine (N.V.D.). **Author contributions:** Conceptualization: Y.D., D.K., Q.H., S.L.C., A.S.B., and P.L. Methodology: B.D., D.K., A.S.B., J.M.S., Y.D., L.E.H., B.T., Q.Z., S.L.C., C.S., Q.H., J.E.F, and A.J.H. Investigation: Y.D., Z.C.Z., Y.Z., D.K., S.L.C., C.S., J.W., J.A.B., L.M.C., L.Y., Z.G.Z. and Q.H. Visualization: Y.D., N.V.D., L.M.C., Q.H., and A.J.H. Validation: Y.D., B.D., A.S.B., S.L.C., C.S., L.M.C., L.Y., Q.H., and A.J.H. Software: N.V.D., J.M.S., J.W., Q.H., and A.J.H. Formal analysis: Y.D., N.V.D., J.M.S., J.W., and A.J.H. Resources: B.D., D.K., Q.Z., and J.A.B. Supervision: P.L., Y.D., Q.Z., and S.L.C. Project administration: B.D., P.L., X.W., L.E.H., Q.Z., S.L.C., and C.S. Funding acquisition: P.L. Writing—original draft: Y.D. and P.L. Writing—review and editing: Y.D., B.D., Y.Z., Q.H., A.J.H., and P.L. **Competing interests:** The authors declare that they have no competing interests. **Data and materials availability:** All data needed to evaluate the conclusions in the paper are present in the paper and/or the Supplementary Materials. RNA-seq data are deposited to GEO under accession number GSE210490.

Submitted 16 February 2024
Accepted 11 September 2024
Published 16 October 2024
10.1126/sciadv.ado7024